The barley mutant *happy under the sun 1* (*hus1*): an additional contribution to pale green crops

Lisa Rotasperti[1†], Luca Tadini[1†], Matteo Chiara[1], Cristina Crosatti[2], Davide Guerra[2], Andrea Tagliani[1], Sara Forlani[1], Ignacio Ezquer[1], David S. Horner[1], Peter Jahns[3], Katarzyna Gajek[4], Addy García[5], Roxana Savin[5], Laura Rossini[6], Alessandro Tondelli[2], Agnieszka Janiak[4], Paolo Pesaresi[1*]

[1] Department of Biosciences, University of Milan, I-20133 Milan, Italy

[2] CREA – Research Centre for Genomics and Bioinformatics, I-29017 Fiorenzuola d'Arda, Italy

[3] Plant Biochemistry, Heinrich Heine University, D-40225 Düsseldorf, Germany

[4] Institute of Biology, Biotechnology and Environmental Protection, University of Silesia in Katowice, P-40-032 Katowice, Poland

[5] Department of Crop and Forest Sciences, University of Lleida - AGROTECNIO Center, Av. R. Roure 191 - S-25198 Lleida, Spain

[6] Department of Agricultural and Environmental Sciences - Production, Landscape, Agroenergy, University of Milan, I-20133 Milan, Italy

[†] These authors contributed equally to the manuscript

* Correspondence to: paolo.pesaresi@unimi.it

Abstract

Truncated antenna size of photosystems and lower leaf chlorophyll content has been shown to increase photosynthetic efficiency and biomass accumulation in microalgae, cyanobacteria and higher plants grown under high-density cultivation conditions. Here, we have asked whether this strategy is also applicable to a major crop by characterising the barley mutant *happy under the sun 1* (*hus1*). The pale green phenotype of *hus1* is due to a 50% reduction in the chlorophyll content of leaves, owing to a premature stop codon in the *HvcpSRP43* gene for the 43-kDa chloroplast Signal Recognition Particle (cpSRP43). The *Hv*cpSRP43 protein is responsible for the uploading of photosystem antenna proteins into the thylakoid membranes, and its truncation results in a smaller photosystem antenna size. Besides a detailed molecular and physiological characterization of the mutant grown under controlled greenhouse conditions, we show that the agronomic performance of *hus1* plants, in terms of total biomass production and grain yield under standard field conditions, is comparable to that of control plants. The results are discussed in terms of the potential benefits of the *hus1* phenotype, and of natural allelic variants of the *HvcpSRP43* locus, with respect to productivity and mitigation of climate change.

Keywords: Photosystem antenna size, Pale green leaves, Photosynthesis efficiency, *Hordeum vulgare*, *Arabidopsis thaliana*

Running head: The pale green *hus1* mutant and the barley yield

Introduction

One of the most urgent challenges faced by plant scientists is to find ways of boosting grain production for human and farm-animal nutrition (Ort *et al.* 2015; Long, Marshall-Colon & Zhu 2015). Meeting this challenge will require the development of crops with increased yield that are able to mitigate the effects of climate change. During the Green Revolution, the yield potential of the major grain crops was raised mainly by increasing the harvest index (HI), which is now higher than 0.5 and close to the biological limit. Therefore, other traits must be explored in order to increase the yield potential of crops further. Modulation of photosynthesis and optimization of solar Energy Conversion Efficiency (ECE) were less extensively studied during the Green Revolution, and still offer significant scope for crop improvement (Long *et al.* 2015; Furbank, Quick & Sirault 2015; Slattery & Ort 2021). It has been estimated that currently attainable levels of ECE (defined as the fraction of absorbed radiation converted into biomass) are equivalent to less than half the theoretical maximum (Slattery & Ort 2015; Slattery & Ort 2021), and several promising targets for its enhancement have already been identified. Of these, truncation of the antenna size of the two photosystems (Kirst & Melis 2013), i.e. decreasing the content of chlorophyll-binding, light-harvesting protein complexes (Lhcs) has proven to be highly effective in the case of high-density cultivation of microalgae (Nakajima & Ueda 1997; Polle, Kanakagiri & Melis 2003; Mussgnug *et al.* 2007) and cyanobacteria (Nakajima & Ueda 1997; Nakajima & Ueda 1999; Kirst, Formighieri & Melis 2014). In these cases, the observed increase in productivity is due to the greater depth of penetration of incident light, together with the reduction of photo-oxidative damage, and of the wasteful dissipation of excess light energy by non-photochemical quenching (NPQ) photo-protective mechanisms (for a review see Melis 2009).

The same arguments apply to crops (Ort *et al.* 2015; Drewry, Kumar & Long 2014; Kirst *et al.* 2018). In general, plants accumulate chlorophyll (Chl) at levels well above the optimum required for maximal growth rate, since their sessile nature makes competition for light and nutrients a major factor for reproductive success (Freschet *et al.* 2011). Thus, while pale green (i.e. low-Chl) plants would lose out in natural competition, they will not pay the same premium as crops, owing to the genetic homogeneity of individual plants and the fact that the canopy density can be fixed at the outset. Indeed, viable mutants with reduced Chl content in leaves and the expected deficiency of Lhc proteins, have been reported in a number of crop plants, including barley (Ghirardi, McCauley & Melis 1986), soybean (Ghirardi & Melis 1988), maize (Greene, Allred, Morishige & Staehelin 1988), sugar beet (Abadia, Glick, Taylor, Terry & Melis 1985), tobacco (Thielen & van Gorkom 1981; Kirst, Gabilly, Niyogi, Lemaux & Melis 2017) and rice (Zhong-wei *et al.* 2016).

However, recent data obtained from both field- and greenhouse-grown Lhc-deficient plants have provided conflicting information on their agronomic performance. In tobacco, for instance, the

reduction in the levels of the light-harvesting complexes of the photosystems in the existing *Su/su* Chl-deficient mutant (Okabe, Schmid & Straub 1977) increased photosynthetic productivity and plant canopy biomass accumulation under high-density cultivation conditions in the greenhouse (Kirst *et al.* 2017; Kirst *et al.* 2018). The same trend was also observed in rice plants with pale-green leaves under high-light conditions (Gu *et al.* 2017).

Conversely, Slattery *et al.* (2017) reported that the $Y_{11}y_{11}$ and y_9y_9 Chl-deficient TLA mutants of soybean (Droppa *et al.* 1998; Ghirardi & Melis 1988) showed a small negative effect on biomass accumulation and yield, in spite of a 50% loss in Chl per unit leaf area. In agreement with these results, the Chl-deficient soybean mutant MinnGold was also reported to exhibit a decrease in total biomass production under field conditions (Sakowska *et al.* 2018; Genesio *et al.* 2020). Similarly, the "Golden" genotype of papaya, characterised by yellowish leaves, showed reduced growth and yield with respect to other genotypes, such as "Sunrise Solo", which has intensely green leaves (Paixão *et al.* 2019). These data indicate that further studies are needed before crops with reduced leaf chlorophyll contents can be usefully exploited for agricultural purposes. Based on these considerations, functional analysis of the diverse genetic loci responsible for pale-green leaf phenotypes in crops has become a priority.

As an example, down-regulation of the nuclear gene for the chloroplast signal recognition particle protein cpSRP43 in *Nicotiana tabacum* resulted in plants with a greater leaf-to-stem ratio, and improved photosynthetic productivity and canopy biomass accumulation under high-density cultivation conditions (Kirst *et al.* 2018). A *cpSRP43* knockout mutant showing the characteristic pale-green phenotype has also been reported in rice (Zhong-wei *et al.* 2016).

cpSRP43 is a chaperone required for post-translational targeting of Lhc to the thylakoid membranes, and contributes to the biogenesis and maintenance of the thylakoid membranes and their associated electron transport chains (Schuenemann *et al.* 1998; Klimyuk *et al.* 1999). The corresponding mutant in *Arabidopsis thaliana* is known as *chaos* [***c***hlorophyll a/b binding protein ***ha***rvesting-***o***rganelle ***s***pecific (Klimyuk *et al.* 1999)]. In the chloroplast stroma, cpSRP43 interacts with cpSRP54 to form the heterodimeric complex cpSRP. Lhc precursors imported into the stroma from the cytosol are N-terminally processed and bound by cpSRP to form a soluble cpSRP-Lhc complex termed the transit complex, which maintains Lhcs in an integration-competent state (for a review see Ziehe, Dünschede & Schünemann 2018). The transit complex is needed to dock and integrate the Lhc proteins into the thylakoid membranes, with the help of the receptor cpFtsY (Kogata, *et al.* 1999; Tu, Schuenemann & Hoffman 1999) and the integral thylakoid membrane protein Alb3, a translocase that physically interacts with cpSRP43 (Moore *et al.* 2000). Recently, cpSRP43 was also shown to efficiently chaperone and stabilize the glutamyl-tRNA reductase (GluTR), a rate-

limiting enzyme in tetrapyrrole biosynthesis, enabling Lhc thylakoid insertion to be coordinated with Chl biosynthesis (Wang *et al.* 2018).

In this work, we report the identification and characterization of a novel pale green barley mutant, named *happy under the sun 1* (*hus1*) for its ability to exhibit a relatively high photosynthetic performance even under high-light conditions. We show that the pale green phenotype is due to a premature stop codon in the *HvcpSRP43* nuclear gene, which disables the chloroplast Signal Recognition Particle 43 kDa (cpSRP43) protein responsible for the uploading of photosystem antenna proteins into the thylakoid membranes. A detailed molecular and physiological characterization of the mutant is provided, together with its performance in terms of total biomass production and grain yield under the different agro-climatic scenarios typical of Central Europe (Modzurow in Silesia, Poland) and Southern Europe (Lleida in Catalonia, Spain), where field trails were carried out during two growing seasons.

Materials and Methods

Nucleotide and Amino acid sequence analysis

The amino-acid sequences of *Hv*cpSRP43 (HUS1), *Hv*cpSRP54-1, *Hv*cpSRP54-2, *At*cpSRP43 and *At*cpSRP54 were obtained from the Barlex (https://apex.ipk-gatersleben.de/apex/f?p=284:10) and UniprotKB (uniprot.org) databases. Multiple sequence alignments were constructed with Clustal Omega (https://www.ebi.ac.uk/Tools/msa/clustalo/) (Sievers *et al.* 2011). Sub-cellular localization and chloroplast transit peptide prediction (cTP) were done with the TargetP algorithm (www.cbs.dtu.dk/services/TargetP). The analysis of nucleotide diversity was carried out using the variant data previously generated by Bustos-Korts et al. (2019). DNASP 5.10.01 software (Librado & Rozas 2009) was used to compute diversity statistics and haplotypes. The haplotype network was drawn using the software PopArt (Leigh & Bryant 2015).

Plant material and growth conditions

Barley (*Hordeum vulgare*) plants were cultivated on acid soil (Vigor plant growth medium, based on Irish and Baltic peats, pH 6.0), supplemented with Osmocote fertilizer, under greenhouse-controlled conditions on a long-day photoperiod (250 µmol photons m^{-2} s^{-1} for 16 h, and 8 h dark). Temperatures were set to 20°C during the day and 16°C at night, with relative humidity of 30%. Before sowing, seeds were treated with Redigo fungicide (Bayer) and incubated at 37°C for 7 days. The *hus1* line was identified as a pale green mutant with improved photosynthetic performance (see section on "Chlorophyll fluorescence measurements and chlorophyll quantification" for further details) in a screen of the M_4 generation of the chemically mutagenized *Hor*TILLUS population (854 mutant families, 20 plants per family; Szurman-Zubrzycka *et al.* 2018) in the 'Sebastian' cultivar background. Nor antibiotic resistance cassette neither any other marker gene is present in the *hus1* line. The F_2 segregating population used to map the *hus1* locus was obtained by crossing the *hus1* mutant with the barley cultivar Morex (six-row; 311 sibling plants used for exome sequencing) and Sebastian (two-row; 346 sibling plants used for segregation analysis). Primers used for the PCR-based segregation analysis are listed in **Table S1**. The *hus1* mutant genetic background was also partially cleaned by backcrossing with Sebastian, and BC_3F_2 plants were used for biochemical and physiological analysis.

The Columbia-0 (Col-0) ecotype of *Arabidopsis thaliana* and the *chaos Enhancer* (*En*) transposon-induced mutant (Tadini *et al.* 2012) were grown on soil in a climate chamber under long-day conditions (150 µmol photons m^{-2} s^{-1} for 16 h, and 8 h dark) at 22°C. To synchronize germination, seeds were first stratified for two days on wet paper at 4°C. The transgenic lines *chaos+35S::hus1-9* and *chaos+35S::HUS1-12* were generated by *Agrobacterium*-mediated transformation of the

Arabidopsis *chaos* mutant with either the barley *hus1* allelic variant or *HvcpSRP43* coding sequence, under the control of the *CaMV 35S* promoter from Cauliflower Mosaic Virus, using the pB2GW7 vector (VIB-UGhent for Plant Systems Biology). Primers used for cloning the coding sequences are listed in **Table S1**.

Field trials and productivity analysis

Five field experiments were conducted in Poland and Spain during two growing seasons, 2017-2018 and 2018-2019. Three experiments were performed in Lleida (Catalonia, Spain - 41°37′00″N, 00°38′00″E, 155 m a.s.l.; with two nitrogen fertilization doses: no nitrogen and 150 kg N ha^{-1} in 2017-2018 and with 150 kg N ha^{-1} in 2018-2019) and two in Modzurow (Silesia, Poland - 50° 16' 15.2688" N, 19° 2' 23.9748" E, 266 m a.s.l.; 60 kg N ha^{-1} in both growing seasons). Two genotypes, *hus1* and the wild type Sebastian, were sown within the optimal sowing dates for the region – i.e. between the end of October and early November in North-Eastern Spain, and during the first week of April in Poland. Sowing rates were 300 seeds m^{-2} in all experiments, i.e. standard density cultivation. Pests, diseases and weeds were prevented or controlled by spraying recommended agrochemicals at the doses suggested by manufacturers or, in the latter case, removed by hand. Each experiment consisted of a randomized complete-block design with two (2017-2018 experiments in Spain) and three (all other experiments) replicates and plots of 5 or 6 m^2 (six rows 4 or 5 m long and 0.17 or 0.20 m apart). In Spain, experiments were conducted under irrigation, in Poland under rain-fed conditions.

Phenological stages were recorded when 50% of the plants in each plot had reached the relevant stage according to the decimal code (Zadoks, Chang & Konzak 1974): heading (DC 59) and maturity (DC 92).

On DC 59 and DC 92, a 1-m long row in the central part of each plot was harvested from the surface of the soil. The area was representative of the whole plot with an adequate density, avoiding borders of the plot or areas already harvested. Total numbers of plants and tillers were also counted. Total biomass was oven-dried for 48 h at 65°C and then weighed. At maturity (DC 92), numbers of spikes were counted, weighed and threshed, and the grains were counted and weighed. Number of grains per m^2 was calculated, together with its components (spikes per m^2 and grains per spike), as well as the average grain weight and the average grain yield.

Exome capture and sequencing

For exome-capture analyses, barley leaf material was collected from 50 F_2 siblings displaying the dark-green leaf phenotype (WT-like pool) and 50 F_2 siblings with the pale-green leaf phenotype (*hus1* pool) derived from the offspring of the *hus1* x Morex cross (see also **Figure S1**). Equal amounts of

leaf tissue from 50 plants for each phenotype were used to extract DNA. DNA was then pooled to form a mutant and a wild-type DNA bulk (Mascher *et al.* 2014). The paired-end exome-capture libraries for Illumina sequencing were prepared using the KAPA High-Throughput Library Preparation Kit, the SeqCap Adapter Kit A with TrueSeq Index Adapters (Roche) and dedicated SeqCap EZ Reagent Kits (Roche). The exome-capture probes were synthetized according to the SeqCap EZ Developer probe pool design 120426_Barley_BEC_D04.EZ, as described by Mascher *et al*. (2013). Aliquots (700 ng) of purified DNA from each of the two F_2 pools were digested enzymatically with the KAPA Fragmentation Enzyme Mix (37°C, 25 min) to obtain fragments ranging from 250 to 350 bp in size. The digestion was followed by end repair using the KAPA End Repair/A-tailing Enzyme Mix, and the index adapters were then ligated to the restriction fragments. Each such mixture was incubated for 15 min at 20°C and then purified using a dual-size selection with AMPure beads (Beckman Coulter) to obtain fragments larger than 250 bp. Then, a pre-capture LM-PCR (ligation–mediated PCR) reaction was performed to enrich the libraries, followed by their purification using AMPure beads. The size ranges of the pre-capture LM-PCR libraries were examined using the Agilent 2100 Bioanalyzer DNA 1000 Chip. Prior to hybridization with exome capture probes, 1 μg of pre-capture LM-PCR library was mixed with 10 μl of SeqCap Developer Reagent (Roche), and 1 μl of SeqCap HE Universal Oligo was added to block the universal segment of library adapters during the hybridization, together with 10 μl of SeqCap HE Index Oligo to block the index segment of library adapter. Next, AMPure beads were added to immobilize the LM-PCR library fragments and later re-suspended in 10.5 μl of the hybridization mixture (SeqCap EZ Hybridization & Wash Kit, Roche). The library was then combined with the SeqCap EZ Probe Pool containing barley exome-capture probes, and allowed to hybridize at 47°C for about 18 h. Afterwards, the hybridized fragments were recovered using Capture Beads (SeqCap EZ Pure Capture Bead Kit, Roche) and subjected to a series of washes of decreasing stringency. The libraries were then amplified using dedicated oligos (SeqCap EZ Accessory Kit v2, Roche), purified using AMPure beads and suspended in 50 μl of 10 mM Tris-HCl. The size ranges of exome capture fragments were analyzed using the Agilent 2100 Bioanalyzer DNA 1000 Chip as described above, the A260/A280 ratio (1.7–2.0) was analyzed on a NanoDrop1000 spectrophotometer and the library was quantified using qPCR with the KAPA Library Quantification Kit (Roche), according to the manufacturer's protocol. The Post-Capture LM-PCR libraries were then subjected to paired-end sequencing on an Illumina HiSeq4000 instrument, using the HiSeq 3000/4000 PE Cluster Kit and the HiSeq 3000/4000 SBS Kit (Illumina), according to the manufacturer's protocol.

Read mapping, data visualization and functional annotation

Reads (2 × 100 bp) of the mutant and wild-type pools were mapped to the second version of the reference genome assembly of barley cv. Morex (Monat *et al.* 2019) using BWA (Li & Durbin 2009) version 0.6.2 (commands 'aln' and 'sampe') software. Variant calling was performed, independently for each pool, with Freebayes version 1.2.0-2 (Garrison & Marth 2012). Reads with a mapping quality (MAPQ score) lower than 20 were discarded (-m 20), and only positions covered by at least 10 reads were considered (--min-coverage 10). Allele frequencies in both pools were calculated as the number of reads supporting a genetic variant divided by the total number of mapped reads by applying a customized Perl script. Variants with allele frequencies ≥80% in both pools were discarded. Bins of 50 polymorphic sites were computed and average allele frequencies were recorded using a customized Perl script. Distribution of allele frequencies along the barley cv. Morex genome assembly were visualized using the standard libraries of the R programming language (R Core Team 2018). Annotation of genetic variants for the prediction of potential functional effects on coding sequences was performed by means of the SNPeff program (Cingolani *et al.* 2012) using the reference annotation of the Morex V2 assembly obtained from https://search.datacite.org/works/10.5447/ipk/2019/8.

RNA extraction, cDNA synthesis and qRT-PCR expression analysis

Total RNA was extracted from leaves as described previously (Verwoerd, Dekker & Hoekema 1989). To remove genomic DNA contamination, TURBO™ DNase (Invitrogen™) was used according to the manufacturer's instructions. The RNA was reverse-transcribed using the iScript™ gDNA Clear cDNA Synthesis Kit (Biorad) and the cDNA was used as the template in qRT-PCRs. qRT-PCR was carried out on a CFX96 Real-Time system (Bio-Rad), using the primer pairs reported in **Table S1**. *HvACTIN 7* (*HORVU.MOREX.r2.1HG0001540.1*) and *PP2A* (*AT1G13320*) were chosen as reference housekeeping genes for barley and Arabidopsis, respectively. The Bio-Rad CFX Maestro 2.0 Software was used to analyze data from three biological and three technical replicates.

PAGE and immunoblot analyses

Thylakoids were prepared from barley leaves collected from 2-week-old seedlings as described previously (Bassi, Peruffo, Barbato & June 1985). Thylakoid proteins isolated from equal amounts of leaf material (fresh weight) were fractionated on denaturing Tris-glycine SDS-PAGE gels (with 12% PAA) and the protein content was stained with Coomassie Brilliant Blue (R250). For

immunoblot analyses, total proteins were extracted from leaves (Martínez-García, Monte & Quail 1999), then fractionated by SDS-PAGE (on 12% polyacrylamide gels) (Schägger & von Jagow 1987). Subsequently, proteins were transferred to poly(vinylidene difluoride) membranes (Ihnatowicz *et al.* 2004), and three replicate filters were probed with specific antibodies. Signals were detected by enhanced chemiluminescence (GE Healthcare) and quantified by ImageJ relative to wild type (= 100%). Thylakoid protein phosphorylation was monitored with a phosphothreonine-specific antibody (Cell Signaling Technology) in total leaf protein extracts obtained from plants kept overnight in the dark and then exposed to light (80 μmol photons m^{-2} s^{-1}) for 4 h.

Antibodies directed against Lhca1 (AS01 005), Lhca3 (AS01 007), Lhcb1 (AS01 004), Lhcb2 (AS01 003), Lhcb3 (AS01 002), Lhcb4 (AS04 045), Lhcb5 (AS01 009), Lhcb6 (AS 01 010), D2 (AS06 146), CP47 (AS04 038), PsaA (AS06172), PsaD (AS09461), RbcL (AS03 037), AtpB (AS05085), PetA (AS08 306), PetB (AS18 4169), PetC (AS08330), PsbO (AS05092), PC (AS06141), PsbS (AS09533) were obtained from Agrisera. P-ThR was purchased from Cell Signaling #9381. The *At*cpSRP43 specific antibody was kindly provided by Laurent Nussaume (Klimyuk *et al.*, 1999).

Chlorophyll fluorescence measurements and chlorophyll quantification

In vivo Chl a fluorescence was recorded on second barley leaves with a Dual PAM 100 (Walz, Effeltrich, Germany) after 30 min of dark adaptation (Barbato *et al.* 2020). Three plants of each genotype for three replicates were analyzed and average values plus/minus standard deviations were calculated. An imaging Chl fluorometer (Imaging PAM; Walz) was used to measure *in vivo* Chl a fluorescence. Dark-adapted plants were exposed to the blue measuring beam (1 Hz, intensity 4; F_0) and a saturating light flash (intensity 4) to obtain F_V/F_M. A 5-min exposure to actinic light (36 μmol photons m^{-2} s^{-1}) was then used to calculate Φ_{II}. The Handy PEA fluorometer (Hansatech Instruments Ltd., UK) was used to measure F_V/F_M and Φ_{II} values in barley plants grown under field conditions during the screening of the *Hor*TILLUS population, and under greenhouse conditions. State transitions were measured with the Dual PAM 100 (Walz, Effeltrich, Germany) as described by Jensen *et al*., (2000).

For Chl quantification, fresh leaves were ground in liquid nitrogen and extracted with 90% acetone. Chl a and b concentrations were measured by spectrophotometry according to Porra *et al*. (1989) and normalized relative to fresh leaf weight. Leaf pigment content was also analyzed in barley and Arabidopsis samples by reversed-phase HPLC (Färber *et al*., 1997). Measurements were performed on five biological replicates for each genotype.

TEM (Transmission Electron Microscopy)

TEM analyses were performed according to Tadini *et al.* (2020). Barley (*HUS1*, *hus1*) and *Arabidopsis thaliana* (Col-0, *chaos*) second-leaf fragments (2 mm x 3 mm) were manually dissected and fixed in 2.5% glutaraldehyde in 0.1 M sodium cacodylate buffer, placed in a vacuum desiccator for 4 h at room temperature and incubated overnight at 4°C. Samples were rinsed twice with 0.1 M sodium cacodylate buffer for 10 min each, and post-fixed in 1% osmium tetroxide in 0.1 M cacodylate buffer for 2 h at 4°C. After two washes with double-distilled water (ddH2O), samples were counterstained with 0.5% uranyl acetate in ddH2O overnight at 4°C in the dark. After rinsing with ddH2O, the tissues were dehydrated by successive immersions in increasing concentrations of ethanol (70%, 80%, 90%) for 10 min each. Subsequently, the samples were dehydrated twice with 100% ethanol for 15 min each. The tissues were then permeated twice with 100% propylene oxide for 15 min. Meanwhile, Epon-Araldite resin was prepared mixing properly Embed-812, Araldite 502, dodecenylsuccinic anhydride (DDSA) and Epon Accelerator DMP-30 according to the manufacturer's specifications. Samples were gradually infiltrated first with a 1:2 mixture of Epon-Araldite and propylene oxide for 2 h, then with Epon-Araldite and propylene oxide (1:1) for 1 h, and left in a 2:1 mixture of Epon-Araldite and propylene oxide overnight at room temperature. Finally, the samples were incubated in pure resin before polymerization at 60°C for 48 h. Resin-embedded samples were cut with an ultramicrotome (PowerTome XL, RMC) into semi-thin sections of 0.5 µm thickness with a glass knife, stained with 0.1% toluidine blue in 0.1 M sodium phosphate buffer and observed with an optical microscope to identify the region of the sample to be investigated at the ultrastructural level. Ultra-thin sections of 70 nm were then cut with a diamond knife (Ultra 45°, DIATOME) and collected on copper grids (G300-Cu, Electron Microscopy Sciences). Samples were observed by transmission electron microscopy (Talos L120C, Thermo Fisher Scientific) at 120 kV and images were acquired with a digital camera (Ceta CMOS Camera, Thermo Fisher Scientific).

Yeast two-hybrid (Y2H) assay

For yeast two-hybrid analyses, the *HvcpSRP43* wild type and the mutated allelic variant (*Hvhus1*) were cloned into pGADT7 (AD-Vector-Clontech) via EcoRI-HF and XhoI restriction sites, while a single EcoRI-HF digest was used for insertion into the pGBKTP7 (BD-Vector-Clontech) vector. *HvcpSRP54* was cloned into the pGADT7 plasmid using EcoRI-HF and SacI-HF sites, while for the pGBKT7 a single EcoRI-HF digestion was used. Primers used for cloning are listed in **Table S1**. The *Saccharomyces cerevisiae* strain AH109 (Clontech Laboratories, Palo Alto, CA, USA) was inoculated into 25 ml of liquid medium (20 g/l yeast extract, 40 g/l tryptone) containing 2% (v/v) of glucose, and incubated overnight at 28°C. The culture was then diluted to a total volume of 150 ml of liquid medium containing glucose and grown for 2 h. The cells were spun down in the centrifuge

for 10 min at 3000 g. After centrifugation, the supernatant was removed and the cells were washed with 1 ml of sterile deionized water. The cells were centrifuged for 10 min at 3000 g and the pellet washed in 1 ml of LiTe buffer (10 mM Tris-HCl pH 7.5, 1 mM EDTA pH 8, 100 mM LiAc). The centrifugation step was repeated and the pellet was resuspended in 100 µl LiTe buffer. For co-transformation 25 µl of the washed yeast cells, 1 µg of each construct, 20 µl of carrier DNA (DNA from fish sperm 2 mg/ml), 20 µl dimethylsulfoxide (DMSO) and 300 µl LiTePEG (10 mM Tris-HCl pH 7.5, 1 mM EDTA pH 8, 100 mM LiAc, 40% PEG v/v) were combined. These preparations were incubated for 30 min at 30°C and for 15 min at 42°C. Cells were then centrifuged for 10 min at 3000 g, resuspended in 100 µl of sterile ddH2O and plated on permissive SC-Drop-Out (-W-L) medium. Afterwards, a few colonies were streaked out on selective SC-Drop-Out (-W-L-H) medium. For semi-quantitative analyses, colonies grown on permissive SC-Drop-Out (-W-L) were inoculated into 10 ml of liquid SC-Drop-Out (-W-L) medium overnight. The cells were then grown on SC-Drop-Out (-W-L-H) and SC-Drop-Out (-W-L-H + 10 mM 3-amino-1,2,4-triazole (AT)) media. The SC-Drop-Out media were prepared with 6.67 g/l yeast nitrogen base (w/o amino acids), 20 g/l glucose, and 0.83 g/l of the appropriate Synthetic Complete Drop-Out Mix (-W-L/ -W-L-H/-W-L-H + 10 mM 3-AT, pH 5.6). All Y2H assays were performed in triplicates.

Virus-Induced Gene Silencing

Transient down-regulation of the *HUS1* locus in the cv. Black Hulless was achieved by virus-induced gene silencing (VIGS), using the modified tripartite genome of the RNA Barley Stripe Mosaic Virus (BSMV) (Palomar, Brakke & Jackson 1977) as described by Holzberg *et al.* (2002). The primers used to amplify a 300-nt fragment of the *HUS1* gene and clone it in the antisense orientation are listed in **Table S1.** The PCR product obtained from the cDNA of the second leaf of Sebastian was cloned into the pBSMV (γ.bPDS4-as) vector after removing the *PDS* (*Phytoene desaturase*) antisense fragment. Plasmids containing the three components of the BSMV genome were linearized with *Mlu*I (α and γ), *Spe*I (βΔβa) and *Bss*HII (γ.bPDS4-as and γ.HUS1-as) before in-vitro transcription with the mMessage mMachine Transcription Kit (Ambion). Transcripts of each of the BSMV genomes were mixed in a 1:1:1 ratio (2.5 µl of each) and combined with 45 µl of FES (Pogue, Lindbo, Dawson & Turpen 1998) obtaining the wild-type virus $BSMV_{WT}$ (α::β.Δβa::γ), and the recombinant viruses $BSMV_{asPDS}$ (α::β.Δβa::γ.bPDS4-as) and $BSMV_{asHUS1}$ (α::β.Δβa::γHUS1-as). A freshly prepared FES/transcript mix for each of the three recombinant viruses was rubbed on the young second leaf of ten Black Hulless barley plants using forefinger and thumb. In addition, 10 plants which were not treated served as controls (Mock). After the inoculation, the plants were grown at 26°C in a growth

chamber to facilitate viral infection. *PDS* and *HUS1* gene silencing was observed and analyzed at 14-17 days post-inoculation (dpi). Three biological replicates were analyzed.

Results

Phenotypic characteristics of the barley pale-green mutant *hus1*

The M_4 generation of the chemically mutagenized barley population *Hor*TILLUS, which originated from the spring cultivar Sebastian (Szurman-Zubrzycka *et al.* 2018), was screened for pale-green leaf mutants with enhanced photosynthetic performance. Of 854 mutant families (20 plants per family) grown at the University of Silesia's Experimental Station in Katowice (Poland), the mutant line 283/001/7/1 was selected since it had the desired traits – i.e. pale-green colour of leaves and increased effective quantum yield of photosystem II (Φ_{II}) under both low (Sebastian, 0.78 ± 0.01 *vs* line 283/001/7/1, 0.82 ± 0.01) and high (Sebastian, 0.53 ± 0.02 *vs* line 283/001/7/1, 0.62 ± 0.01) light levels. Because of its relatively high photosynthetic efficiency under high-light conditions, the mutant line was renamed *happy under the sun 1* (*hus1*). In order to reduce the number of chemically induced mutations in the genome, the *hus1* mutant was backcrossed with the barley cv. Sebastian, and BC_3F_2 plants showing the *hus1* phenotype were selected for detailed biochemical and physiological characterization, together with their wild-type-like siblings (referred to as *HUS1* in the following). Under greenhouse growth conditions, *hus1* plants are characterised by a wild-type-like growth rate, when compared to *HUS1* as control (**Figure 1A**). Analysis of the leaf pigment content revealed a reduction of about 50% in total chlorophyll (Chl a+b) in *hus1* relative to *HUS1*. Furthermore, the *hus1* Chl a/b ratio was increased to about 4.1, while *HUS1* leaves displayed a Chl a/b ratio of 3.3. The latter is typical for the fully developed photosynthetic apparatus in green leaves (Masuda & Melis 2002), whereas the substantially higher Chl a/Chl b ratio in *hus1* leaves suggested a smaller photosystem antenna size (Melis 1991) (**Figure 1B**). To substantiate this finding, thylakoid proteins were extracted from equal amounts of *HUS1* and *hus1* leaves, fractionated by SDS-PAGE, and stained with Coomassie Brilliant Blue (C.B.B.). In agreement with the leaf chlorophyll content, the pattern obtained for the *hus1* sample showed a marked reduction of proteins in the region between 20 and 25 kDa, where the antenna proteins of both photosystems, i.e. Lhca (light-harvesting complexes associated with photosystem I - PSI) and Lhcb (light-harvesting complexes associated with photosystem II - PSII), are expected to migrate (**Figure 1C**). In order to assess their photosynthetic performance, dark-adapted *HUS1* and *hus1* leaves were exposed to increasing actinic light intensities (0 to 1287 μmol photons m^{-2} s^{-1}) and the parameters Φ_{II} and Y(NPQ) (the quantum yield of regulated energy dissipation of PSII) were measured. Under increasing actinic light levels, the concomitant decrease of Φ_{II} and increase of Y(NPQ) values were shifted towards higher light intensities in *hus1* with respect to *HUS1* leaves. (**Figure 1D-E**). This is compatible with the reduction in the size of the functional antenna in *hus1* thylakoids, since *hus1* leaves need higher light intensities to reach the same values for electron transport rate and luminal pH as the *HUS1* control.

Exome sequencing and *hus1* locus identification

In order to map the *hus1* locus, a segregating F_2 population of 311 plants was generated by crossing the *hus1* mutant (background Sebastian) with the cv. Morex, whose genome has been fully sequenced and annotated (Monat *et al.* 2019). Around 1/4 of the total population (73/311) were *hus1*-like plants, with the characteristic pale-green phenotype and increased Φ_{II} values – indicating that *hus1* is a monogenic recessive trait (**Figure S1A**). Subsequently, genomic DNA was isolated from 50 F_2 siblings showing the wild-type dark-green leaf phenotype and 50 F_2 siblings with the *hus1* phenotype (**Figure S1B**) and bulked in equal ratio to generate two different DNA pools. Both DNA pools were subjected to exome capture (Mascher *et al.* 2013) (see Materials and Methods for details) and paired-end sequencing, yielding for each pool approximately 80 million 2x100-bp read pairs. Reads were then mapped onto the reference genome assembly for cv. Morex (Monat *et al.* 2019) and genetic variants were identified. Visualization of the allele frequencies at SNP positions along the barley genome sequence revealed a single sharp peak on the long arm of chromosome 4H, highlighting a candidate region of 4.5 Mbp (from 598769958 bp to 603280034 bp), where the two pools were mostly heterogeneous – i.e. the frequency of the mutant allele increased to over 97% in the *hus1*-like pool and dropped to about 30% in the WT-like pool (**Figure 2A**). Within this region, only one locus - the single-copy *HORVU.MOREX.r2.4HG0341350* gene - carried a "highly damaging" mutation: a G-to-A transition at position c. 885 (position 885 in the cds), as predicted by the SNPeff software, resulting in a premature stop-codon, at residue Tryprophan-295 (**Figure 2B**; see also **Supplementary Data**). The *HORVU.MOREX.r2.4HG0341350* product was predicted by TargetP-2.0 (http://www.cbs.dtu.dk/services/TargetP/) to encode a protein carrying a 56 a.a. chloroplast transit peptide (cTP) at the N-terminus (**Figure 2B**), and to be highly expressed in shoots, according to Barlex database (https://apex.ipk-gatersleben.de/apex/f?p=284:49:::::P49_GENE_CHOICE:4; see also **Supplementary Data**).

To further investigate the possible association of the nonsense mutation with the *hus1* phenotype, an F_2 segregating population of 346 plants was generated by backcrossing *hus1* with the control cv. Sebastian. PCR-based amplification and sequencing of the *HORVU.MOREX.r2.4HG0341350* gene revealed that plants showing the wild-type dark-green leaf phenotype were either homozygous (88 plants) or heterozygous (174 plants) for the wild-type allele – i.e. with a G in position 885 – while the pale-green *hus1* plants (84 plants) were all homozygous for the mutated allele, carrying an A in position 885 (**Figure 2C**). Furthermore, quantitative real-time

PCR (qRT-PCR) analysis revealed a reduction of about 90% in *HORVU.MOREX.R2.4HG0341350* transcripts in *hus1* leaves with respect to *HUS1* (**Figure 2D**).

To support the association between the altered expression of *HUS1* and the pale-green barley phenotype with independent evidence, a *HUS1* virus-induced gene silencing (VIGS) assay was performed in the cv. Black Hulless, using the barley stripe mosaic virus (BSMV; Holzberg *et al.* 2002). The tripartite genome of BSMV was modified to express partial cDNAs (around 300 nt) corresponding to *HUS1* (BSMV$_{asHUS1}$) and *PDS* (a phytoene desaturase used as the positive control; BSMV$_{asPDS}$) genes in antisense orientation (**Figure 3**). Black Hulless leaves infected with BSMV expressing the barley PDS fragment in antisense orientation were photo-bleached by 14 days post-inoculation (dpi) and resembled plants treated with norflurazon, a chemical inhibitor of the PDS enzyme. On the other hand, barley leaves infected with BSMV$_{asHUS1}$ showed a pale-green phenotype after 14 dpi, similar to that of *hus1* leaves. Conversely, barley infected with the non-modified BSMV (BSMV$_{WT}$) or subjected to mock infection showed neither photo-bleaching nor reduced leaf chlorophyll content (**Figure 3A**). Imaging PAM-based Φ_{II} measurements showed that values for mock-treated, BSMV$_{WT}$- and BSMV$_{asHUS1}$-infected leaves were comparable to each other, while BSMV$_{asPDS}$ samples exhibited a drastic reduction in photosynthetic efficiency (**Figure 3A**). Moreover, gene expression analysis conducted by qRT-PCR revealed a reduction of about 50% in the level of *HUS1* mRNA in barley leaves infected with BSMV$_{asHUS1}$ (**Figure 3B**). As a consequence, BSMV$_{asHUS1}$ displayed a marked reduction in amounts of Lhcb1, Lhcb3 and Lhca3 proteins, while the levels of Lhcb2 and Lhcb5 proteins in BSMV$_{asHUS1}$-infected and control samples were similar to each other, supporting a specific decrease in antenna protein accumulation like that observed in *hus1* leaves (**Figure 3C**). The slightly different Φ_{II} values found for BSMV$_{asHUS1}$-infected and *hus1* leaves can be attributed to the less severe reduction in *HUS1* gene expression in the former (about 50% as against 90% in *hus1*) and to the stripe phenotype of BSMV$_{asHUS1}$-infected leaves relative to *hus1* samples.

Taken together, these independent lines of evidence strongly support the identification of *HORVU.MOREX.R2.4HG0341350* as the locus targeted in the *hus1* mutant.

HORVU.MOREX.R2.4HG0341350 encodes the chloroplast 43-kDa Signal Recognition Particle protein - *Hv*cpSRP43

Conceptual translation of the protein encoded by the *HORVU.MOREX.r2.4HG0341350* gene shows 48% identity and 62% similarity to the *Arabidopsis thaliana At*cpSRP43 (Signal recognition particle 43-kDa protein; Klimyuk *et al.* 1999). This protein, which is encoded by a single-copy gene in both barley and Arabidopsis, is unique to plants, and contains a typical chloroplast transit peptide at the N-terminus and two discrete domains that mediate protein-protein interactions (**Figure S2**). The first domain comprises four ankyrin repeats in tandem (ANK1-4). Ankyrin repeats are found in a very large number of proteins, and they generate dimerization interfaces for a variety of different protein substrates. The second domain shows similarity to the chromatin-binding domain (chromodomain), first identified in the Drosophila proteins Polycomb and heterochromatin protein 1 (Paro & Hogness 1991). In the cpSPR43 protein two chromodomains in tandem span the C-terminal region, and a third chromodomain is located near the N-terminus of the mature protein (CD1-3). CD2 and CD3 have been reported to be strictly required for the stable formation of the cpSRP43-cpSRP54 heterodimer, even in the absence of Lhc proteins (Groves *et al.* 2001; Funke, Knechten, Ollesch & Schu 2005), while the four ANK domains, together with CD1, form the binding domain that protects Lhc proteins from aggregation in an aqueous milieu (for a review see Ziehe *et al.* 2018). Strikingly, the premature stop codon in the *hus1* mutant allele truncates CD2 and deletes CD3, presumably preventing formation of the cpSRP43-cpSRP54 heterodimer and thus blocking access of Lhc proteins to the thylakoids (**Figure S2**).

In order to determine whether the barley *HUS1* locus is the functional homologue of Arabidopsis *cpSRP43* gene, also known as *CAO* (*At2g47450*), a comparative characterization of barley *hus1* and the Arabidopsis knockout mutant *cpsrp43/chaos* was carried out, using *HUS1* and Columbia-0 (Col-0) as controls for barley and Arabidopsis, respectively (**Table 1** and **Figure 4**).

At first, since both mutants exhibit a markedly pale-green leaf coloration compared to the corresponding controls, the leaf pigment content was quantified by High Performance Liquid Chromatography (HPLC) (**Table 1**). The total Chl content (Chl a+b) was markedly reduced in both pale green mutants, reaching about 47% of *HUS1* content in *hus1* and 68% of the Col-0 amount in *chaos*. Conversely, the Chl a/b ratio was >4:1 in both pale mutants, while the corresponding wild-type plants displayed a Chl a/b ratio of about 3:1, indicating preferential loss of Chl b, which is mainly associated with the antenna proteins of both photosystems. The carotenoid content also differed between wild-type and mutant leaves. In particular, the carotenoids that specifically bind to the antenna proteins of the two photosystems, such as neoxanthin (Nx), lutein (Lut) and the VAZ pool

(violaxanthin + antheraxanthin + zeaxanthin), were markedly reduced in both *hus1* and *chaos* leaves, thus providing further support for the decrease of photosystem antenna size in both mutants. Notably, levels of β-carotene (β-Car), which associates with PSII core proteins, did not vary significantly among the different genotypes. In addition, in both mutants, the pale green phenotype was associated with an increase in photosynthetic performance, as revealed by the higher Φ_{II} values and the increased oxidation levels of the plastoquinone (PQ) pool – i.e. increased qL values (Kramer, Cruz & Kanazawa 2003; Henikoff *et al.* 2004; Tadini *et al.* 2012) as measured with the Imaging-PAM fluorometer (**Figure 4A**).

Subsequently, immunoblots were used to analyse the protein composition of the thylakoid electron transport chain. In agreement with the pigment quantification, a specific decrease in amounts of pigment-binding antenna proteins was observed in *hus1* and *chaos* thylakoids. Some of the antenna complexes of both photosystems, such as Lhcb1, Lhcb2, Lhcb6, Lhca1, Lhca3, accumulated to between 10% and 65% of the corresponding control levels, while Lhcb3 was below the limit of detection in both *hus1* and *chaos* thylakoid membranes (**Figure 4B** and **Table S2**). Conversely, accumulation of Lhcb4 and Lhcb5 was unchanged in the thylakoid membranes of both the barley and the Arabidopsis mutant. As in the case of *chaos*, the *hus1* mutation did not affect the accumulation of photosystem core subunits (D2, CP47, PsaA), the oxygen-evolving complex (PsbO), the PsbS subunit of PSII, cytochrome *b*$_6$*f* (PetA, PetB, PetC), ATPase (AtpB) or plastocyanin (PC). However, the PsaD subunit was clearly affected in the *hus1* genetic background, but not in the *chaos* mutant (**Figure 4B** and **Table S2**). An antibody specific for *At*cpSRP43 protein was also able to show the complete absence of the protein in Arabidopsis *chaos* chloroplasts (**Figure 4C**), while it was unable to detect the barley counterpart. The specific and marked decrease in PSII antenna size was further confirmed by state-transition (ST) measurements, which quantify the phosphorylation-mediated migration of the mobile pool of the PSII light-harvesting complex (P-Lhcb1/b2) between the two photosystems (Jensen *et al.* 2000). In agreement with the phenotype observed in *chaos* (Tadini *et al.* 2012), this process was also effectively abolished in *hus1* thylakoids – as revealed by ST values of 0.016 ± 0.019 (n = 5), in comparison to 0.095 ± 0.014 (n = 5) observed in *HUS1* leaves, and by the complete lack of Lhcb phosphorylation in the leaves of both mutants upon exposure to growth light conditions (**Figure 4D**). This is due to the concomitant reduction in steady-state amounts of Lhcb proteins and the higher level of oxidation of the plastoquinone (PQ) pool observed in both mutants, which together prevent activation of the STN7 kinase (see qL values in **Figure 4A;** Bonardi *et al.* 2005).

Transmission electron microscopy (TEM) analyses were also performed in order to monitor the impact of the decreased photosystem antenna size on the ultrastructure of thylakoid membranes

(**Figure 5**). In this respect also, the barley *hus1* and Arabidopsis *chaos* mutants showed very similar features, including reduced accumulation of starch grains in the chloroplast stroma. Furthermore, the grana stacks (arrowheads) appeared to be thinner in *hus1* chloroplasts than in the *HUS1* control (**Figure 5**).

Finally, to verify the involvement of the *HORVU.MOREX.R2.4HG0341350* gene in uploading of antenna proteins into the thylakoid membranes, the *HORVU.MOREX.R2.4HG0341350* coding sequence (CDS) and the *hus1* mutated allelic variant were cloned into a binary vector, under the control of the *CaMV35S* promoter, and introduced into the Arabidopsis *chaos* genetic background, via Agrobacterium-mediated transformation. Seventeen *chaos+35S::HUS1* T1 lines were obtained, and all of them were able to fully complement the pale-green *chaos* phenotype, restoring the Col-0 pigmentation in cotyledons and true leaves, as well as photosynthetic performance and antenna protein accumulation (**Figure 6**). Conversely, none of the 25 *chaos+35S::hus1* T1 lines examined showed any evidence of rescue of any of the traits investigated (**Figure 6**), despite comparable expression levels of both constructs (**Figure 6C**).

Overall, these data led us to conclude that the barley *HORVU.MOREX.R2.4HG0341350* gene is the functional homologue of the Arabidopsis *cpSRP43/CAO/At2g47450* locus, and that the identified nonsense mutation is the cause of the pale green phenotype observed in *hus1* plants. The *HORVU.MOREX.R2.4HG0341350* gene was therefore renamed *HvcpSRP43*.

*Hv*cpSRP43 interacts physically with barley *Hv*cpSRP54 protein

Under physiological conditions, cpSRP43 interacts with cpSRP54 to form the heterodimeric cpSRP43-cpSRP54 complex required to target and integrate some of the antenna proteins into the thylakoid membranes (Ziehe *et al.* 2018). Hence, we asked whether a similar complex exists in barley. To do so, we used the amino-acid sequence of Arabidopsis cpSRP54 (AtcpSRP54, *At5g03940*) to query the barley *cv* Morex proteome (Monat *et al.* 2019). A BLAST-P search on the IPK Barley BLAST Server identified two putative *Hv*cpSRP54 amino-acid sequences, encoded by *HORVU.MOREX.r2.4HG0293270* (referred to from here on as *HvcpSRP54-1*) and *HORVU.MOREX.r2.4HG0293280* (from here on *HvcpSRP54-2*) genes. As shown in **Figure S3A**, although their cTPs differ considerably, *At*cpSRP54 shares high levels of identity with *Hv*cpSRP54-1 (72%) and *Hv*cpSRP54-2 (76%). Interestingly, the level of expression of *HvcpSRP54-1* in leaves was higher than that of *HvcpSRP54-2*, as monitored by qRT-PCR in the control Sebastian genetic background (**Figure S3B**). Moreover, *HvcpSRP54-1* was found to be strongly down-regulated (to

about 10% of the Sebastian control level) in the *hus1* mutant background, similarly to *HvcpSRP43* transcript levels (**Figure S3C**). Down-regulation of *cpSRP54* gene expression was also observed in the Arabidopsis *chaos* mutant (**Figure S3D**), implying a strict co-regulation of the *cpSRP43* and *cpSRP54* genes in both species.

On the basis of the observed expression patterns, *Hv*cpSRP54-1 was selected as the best candidate for interaction studies with *Hv*cpSRP43, using the yeast two-hybrid (Y2H) assay. The mature coding sequences of *HvcpSRP54-1* and *HvcpSRP43* (i.e. devoid of the cTPs), as well as of the mutated version of *HvcpSRP43* carrying the premature stop codon (*Hvhus1*), were cloned into the pGADT7 and pGBKT7 vectors, downstream of the GAL4 DNA activation domain (AD) and GAL4 DNA-binding domain (BD), respectively, and these constructs were then used to co-transform the *Saccharomyces cerevisiae* strain AH109. After verifying that all the yeast colonies were able to grow on the permissive medium devoid of Trp and Leu (SD -W -L), auto-activation tests were carried out on selective media lacking histidine (SD -W -L -H) either in the absence or presence of 10 mM 3-amino-1,2,4-triazole (3-AT), a competitive inhibitor of the product of the *HIS3* reporter gene. None of the constructs used in the assay exhibited auto-activation, as shown by the total absence of yeast growth on selective medium in the presence of the empty vectors (AD*Ø*, BD*Ø*, **Figure S4**).

The physical interaction between *Hv*cpSRP54-1-AD and *Hv*cpSRP43-BD, as well as between *Hv*cpSRP43-AD and *Hv*cpSRP54-1-BD, was demonstrated by the growth of the doubly transformed yeast cells on selective medium with and without 10 mM 3AT (SD -W-L-H; **Figure 7**), supporting the existence of the heterodimeric cpSRP43-cpSRP54 complex also in barley. Furthermore, the ability of *Hv*cpSRP43 to form homodimers (the yeast strain expressing the *Hv*cpSRP43-AD and *Hv*cpSRP43-BD proteins was able to grow on selective medium) also suggests the possible existence of a heterotrimeric protein complex consisting of two copies of cpSRP43 and one of cpSRP54, as described earlier in Arabidopsis (Tu *et al.* 1999). No interaction between the truncated *Hv*hus1 and *Hv*cpSRP54-1 was detected, while the *Hv*hus1 protein retained the ability to form dimers with itself and with *Hv*cpSRP43. These findings support the notion that the chromodomains CD2 and CD3 at the C-terminus of *Hv*cpSRP43 (**Figure S2**) are essential for recruitment of, and interaction with the cpSRP54 subunit, as previously observed (Jonas-Straube *et al.* 2001; **Figure 7**). On the other hand, the intact ankyrin repeats present in both *Hv*cpSRP43 and *Hv*hus1 proteins retain their ability to homodimerize.

Natural variation of *HvcpSRP43* locus in barley

Natural variation of *HvcpSRP43* was investigated in order to identify natural occurring alleles. To this end, we used exome capture and sequencing data available for the WHEALBI barley collection (Bustos-Korts *et al.* 2019), which includes 403 cultivars, landraces and wild barley accessions originating from a wide range of geographic locations. Overall, 50 single-nucleotide polymorphisms (SNPs) were retrieved in a 1986-bp region spanning the *HUS1* gene, 15 of which fall within the single exon of the gene, while 22 and 13 SNPs map to the 3' and 5' prime regions of the gene, respectively. Of the 15 SNPs in the coding region, 6 were synonymous mutations and 9 missense mutations. Based on polymorphic sites, 44 haplotypes were identified in the collection (**Figure 8**). Eight haplotypes described most of the genotypes (334) in the collection, with 152 accessions belonging to the same haplotype (Hap_34). Haplotype diversity was highest in wild barley (0.97), followed by landraces and, lastly, cultivars (**Table S3**). To verify that the selection of polymorphisms was random, Tajima's D test (Tajima 1989) for neutrality of selection was performed. Tajima's D values never reached significance in any of the tests, indicating that sequence diversity is not due to selection.

Grain yield and biomass accumulation under field conditions

The performance of *hus1* and Sebastian control plants with respect to grain yield and total biomass accumulation, under field conditions, was monitored in Lleida (Spain), representing the south European agroclimatic zone, and in Modzurow (Poland, representing the central European agroclimatic zone). Field experiments were carried out independently in two successive growing seasons, 2017-2018 and 2018-2019, using a fully randomized experimental design (for further details see Materials and Methods; **Figure 9**). Grain yield ranged from approximately 5000 kg ha^{-1}, observed for *hus1* grown in Poland during the growing season 2018-2019, to around 8500 kg ha^{-1} reported for Sebastian in Spain during the growing season 2018-2019, most probably as a consequence of the different weather conditions (**Figure 9A**). However, in none of the field experiments did the grain yields of *hus1* and Sebastian differ significantly from one another. Furthermore, grain yield was strongly correlated with the total biomass at maturity across all experimental conditions (**Figure 9B**; $y = 0.52x - 418.9$; $R^2 = 0.91$, $P<0.001$) and there were no statistically significant differences between the two genotypes in the accumulation of biomass, either at pre-heading or post-heading stages (**Figure 9C**).

Discussion

The pale green hus1 phenotype in barley is caused by a premature stop codon in HORVU.MOREX.R2.4HG0341350 gene

This work makes a contribution to the study of low-Chl-content crops by characterizing *hus1*, a pale green barley mutant that carries a premature stop codon in the single-exon gene *HORVU.MOREX.r2.4HG0341350*, which codes for the protein *Hv*cpSRP43. The mutation results in reduced accumulation of *HvcpSRP43* transcripts, most probably as a consequence of a surveillance pathway known as the Nonsense-Mediated Decay (NMD) pathway, which selectively recognises and degrades mRNAs harbouring premature termination codons (Kervestin & Jacobson 2012; Schweingruber *et al.* 2013). Furthermore, the barley *hus1* and the Arabidopsis knockout *chaos* mutants (see **Figure 4C**) share almost identical visible and molecular phenotypes (this manuscript; see also Klimyuk *et al.* 1999), allowing to assume that a knockout mutation is also responsible for the *hus1* phenotype. Alternatively, even if the truncated version of *Hv*cpSRP43 were not degraded, it would be unable to physically interact with *Hv*cpSRP54, as revealed by the yeast two-hybrid assay (see **Figures 7** and **S4**). This is due to the lack of the C-terminal chromodomains CD2 and CD3, which are essential for the formation of the *Hv*cpSRP43-*Hv*cpSRP54 heterodimer and the cpSRP-Lhc transit complex. As a consequence, antenna proteins of both photosystems, such as Lhcb1, Lhcb2, Lhcb6, Lhca1 and Lhca3, accumulate to lower levels in the thylakoid membranes, while Lhcb3 is below the limit of detection, which is compatible with the markedly reduced chlorophyll content of the leaves. Moreover, the general deficiency of PSII antenna proteins appears to be responsible for the decrease in NPQ activity and the higher effective quantum yield of PSII under diverse light intensities. As already reported by Klennel *et al.* (2005) in Arabidopsis, the *chaos* mutant shows reduced sensitivity to photo-oxidative damage and enhanced recovery rate in young seedlings, compared to the wild-type control. A similar phenotype in terms of total chlorophyll content and chlorophyll a/b ratio was also observed in the *ygl9* (Zhong-wei *et al.* 2016) and *w67* (Lv *et al*. 2015) rice mutants and in *TLA3-RNAi* tobaco plants (Kirst *et al.* 2018), while it differs substantially from *Chlamydomonas reinhardtii cpSRP43*-null mutant, at least in terms of the pigments accumulating in the chloroplast (Kirst *et al.* 2012). In particular, the chlorophyll content in *C. reinhardtii cpSRP43*-null mutant dropped to 15% of that of the wild type (Kirst *et al.* 2012), while barley, rice, Arabidopsis and tobacco *cpSRP43* mutants retained about 50% of wild-type chlorophyll levels (this manuscript; Zhong-wei *et al.* 2016; Lv *et al*. 2015; Klimyuk *et al.* 1999; Kirst *et al.* 2018). This major difference is most probably due to the severe drop of photosystem core protein accumulation observed in *C. reinhardtii cpSRP43* mutant, but not in the corresponding mutants of higher plants.

The pale green hus1 mutant does not show increased biomass accumulation and grain yield under standard field conditions

Recent studies carried out on model organisms have shown that reduced contents of leaf chlorophyll in mutants of cyanobacteria, unicellular algae and land plants can enhance yields, while allowing for higher cultivation densities, thus minimising the surface required for cultivation (Kirst & Melis 2013; Kirts *et al.* 2014; Kirst *et al.* 2017; Kirst *et al.* 2018; Mussgnug *et al.* 2007; Gu *et al.* 2017; Negi *et al.* 2020). Higher-density cultivation also offers additional benefits in crops, as they would achieve canopy closure more rapidly. That would minimize losses of soil moisture, and reduce the amount of fertilizer needed – particularly nitrogen, which is largely used for chlorophyll and antenna protein synthesis – thus minimizing fertilizer runoff. Higher-density would also alleviate the need for herbicides, as rapid and unbroken canopy closure will create the shading needed to suppress the growth of weeds, and decrease the water requirement for growth, since heat production from thermal dissipation of absorbed light (approx. 96-99% in dark green plants) will be lower in pale green plants and less transpiration will be required for thermoregulation.

Consistently with previous reports (Slattery *et al.* 2017; Sakowska *et al.* 2018; Gu *et al.* 2018; Genesio *et al.* 2020), the *hus1* mutant accumulated biomass and grains at levels comparable to those observed for the control cultivar Sebastian, when grown under field conditions under standard density cultivation (300 seeds m^{-2}, see also Materials and Methods) in Spain and Poland. Actually, *hus1* plants showed, on average, a slight reduction in grain yield and biomass accumulation (relative to the wild-type control) in all field experiments (**Figure 9**), which was more evident at the post-heading stage (i.e. during seed filling) than at the pre-heading stage, where the total biomass accumulation was identical to that of the control (see **Figure 9C**). This suggests a possible reduction in the sink capacity in *hus1* plants. Alternatively, pale green flag leaves and ears could be associated with source limitation during grain filling.

However, the *hus1* mutant performed much better than the yellow soybean mutant, MinnGold, characterised by a reduction of about 30% in leaf biomass accumulation with respect to the two green soybean varieties used as control (Sakowska *et al.* 2018). Interestingly, this soybean mutant is characterised by a greater reduction in leaf chlorophyll content (80%) than that seen in *hus1* leaves (50%), indicating that a threshold limit may exist below which reduction of chlorophyll levels in the leaves becomes a limiting factor. This is in agreement with the prediction of the WIMOVAC sun-shade model according to which reducing chlorophyll content by half could increase canopy carbon gains, but further reductions in chlorophyll would be disadvantageous (Ort *et al.* 2011). Nevertheless, it is worth mentioning that the MinnGold mutation is caused by a nonsynonymous nucleotide

substitution in the third exon of a Mg-chelatase subunit gene (ChlI1a) on chromosome 13 (Campbell *et al.* 2015). The mutant might accumulate protoporphyrin IX, a strong photosensitizer chaotropic compound that would lead to photobleaching in a light-intensity dependent manner. Furthermore, mutations in subunit I of magnesium chelatase might have an impact in abscisic acid signalling and stomatal movement (Du et al. 2012; Tomiyama et al. 2014). Therefore, the MinnGold mutation could negatively affect yield thorough both increased photooxidative damages and soil water depletion, especially when drought conditions occur during key developmental stages (Slattery *et al.* 2017), rather than through the reduced leaf chlorophyll content.

Besides the possible advantages for productivity and efficiency of resource use, the introduction of novel low-Chl-content crops might also be of critical importance in climate change mitigation since it should increase the surface albedo, i.e. the ratio of reflected to incoming short-wave irradiance. In particular, the expected reduction of greenhouse gas (GHG) emissions may lead to an increase in solar irradiance and air warming, with the consequent occurrence of heatwaves and an increase in the evaporative demand of the atmosphere (Genesio *et al.* 2020). New crops with low-Chl-content might represent a sustainable and, relatively simple, solution to reduce solar irradiance by increasing the surface reflectance of large geographical areas. Modelling experiments have, indeed, repeatedly shown that higher cropland albedo may effectively mitigate the magnitude of future heatwaves and global warming in general (Ridgwell, Singarayer, Hetherington & Valdes 2009; Zamft & Conrado 2015) by lowering near-surface air temperatures (Seneviratne *et al.* 2018).

On the basis of these considerations, the *hus1* mutant deserves further analyses under field conditions, possibly at higher densities of cultivation, to verify whether the major potential advantages predicted for pale-green crops, such as increased productivity, improved resource use efficiency and climate change mitigation, i.e. increased albedo, also apply to the *hus1* genetic background.

The hus1 mutant and natural alleles of HvcpSRP43 locus could make an important contribution towards a new generation of pale green crops

The domestication of crops characterised by low Chl contents, high yield and a strong capacity for photoprotection against high irradiance requires a detailed functional genomic analysis of the major loci involved in leaf Chl accumulation, and their introgression into elite material. Furthermore, the differential impacts of this new generation of crops in different areas of the world needs to be evaluated, since it depends, for instance, on the local/seasonal irradiance. In relation to that, barley

represents an ideal model species for functional genomics studies, given the large collections of mutant populations, a complete genome assembly and protocols for genetic transformation and gene editing, and the availability of a large range of natural genetic diversity (Rotasperti, Sansoni, Mizzotti, Tadini & Pesaresi 2020).

For instance, the natural allelic variants of *HvcpSRP43* gene identified within the WHEALBI collection (http://www.whealbi.eu/; (Bustos-Korts *et al.* 2019) might represent an invaluable genetic resource for the investigation of how leaf chlorophyll content adapts to the different agro-climatic scenarios worldwide. As a matter of fact, the *hus1* mutation led to a marked drop in leaf chlorophyll content, while natural, SNP-induced single amino-acid exchanges might fine-tune amounts of leaf chlorophyll to specific environmental conditions.

It is worth noting that, given the high level of conservation of the photosynthetic apparatus among higher plants, this knowledge could be transferred to other crop species, providing room for yield increase, while minimizing the space and resources needed for cultivation. Furthermore, soybean, corn and wheat (among other crops) with reduced leaf chlorophyll contents could represent a sustainable solution to some of the problems associated with mitigation of climate change.

Acknowledgements

This project was supported by ERA-NET Cofund FACCE SURPLUS (BarPLUS grant id. 93) funded by MIUR to PP, by MIPAAF to AT and by FACCE SURPLUS/I/BARPLUS/05/2016 (funded by the National Centre for Research and Development in Poland) to AJ. We are also grateful to MIUR-PRIN 2017FBS8YN to PP. The NoLimits platform at University of Milano is acknowledged for the TEM analysis. We are also grateful to Laurent Nussaume for providing us with the *At*cpSRP43 antibody. This manuscript is dedicated to the memory of Prof. Michele Stanca, a world-renowned scientist, who transmitted his passion for cereal genetics to many of the scientists that co-authored this article. Paul Hardy is also acknowledged for critical reading of the manuscript.

Author contributions

LiRo, LT and PP designed the study. LiRo, LT, KG, AJ, and PP took care of isolation of *hus1* mutant. LiRo, LT, SF, IE, PJ, AJ were responsible of the molecular biology, biochemical and physiological characterization of mutants. LiRo and AT contributed to the yeast two-hybrid assay. LiRo and LT were responsible of the TEM images. LiRo, KG and AJ performed Exome sequencing. MC, DH and LaRo took care of exome sequencing data analysis and identification of *hus1* locus. LiRo, CC, AT were responsible of VIGS assay. AG, RS, AT, KG and AJ conducted the field trials. All authors helped draft the manuscript. PP coordinated the study and took care of the final version of the manuscript. All authors gave final approval for publication and agree to be held accountable for the work performed therein.

Conflicts of interest

The authors declare no conflicts of interest.

Table 1. HPLC analysis of pigment content in Sebastian, *hus1*, Col-0 and *chaos* leaves. Pigment quantification is reported in pmol per mg fresh weight (FW). Nx, neoxanthin; Vx, violaxanthin; Lut, lutein; Chl, chlorophyll; VAZ, violaxanthin + antheraxanthin + zeaxanthin; β-Car, β-carotene. Student's t-test, $**P<0.01$, $***P<0.001$, ns = not significant.

	Nx	Vx	Lut	Chl b	Chl a	β-Car	VAZ	Chl a/b	Chl a+b
HUS1	90±12	123±20	249±27	774±54	2579±271	97±32	132 ± 22	3.33±0.129	3353±325
hus1	32±4***	74±20**	92±21***	311±23***	1253±105***	121±67	83±23**	4.03±0.108***	1564±128***
Col-0	45±4	50±4	146±25	359±36	1141±106	84±30	52±4	3.18±0.036	1500±142
chaos	22±1***	40±4**	90±11**	200±10***	826±50***	92±27	43±5**	4.13±0.047***	1026±60***

Figures and Figure legends

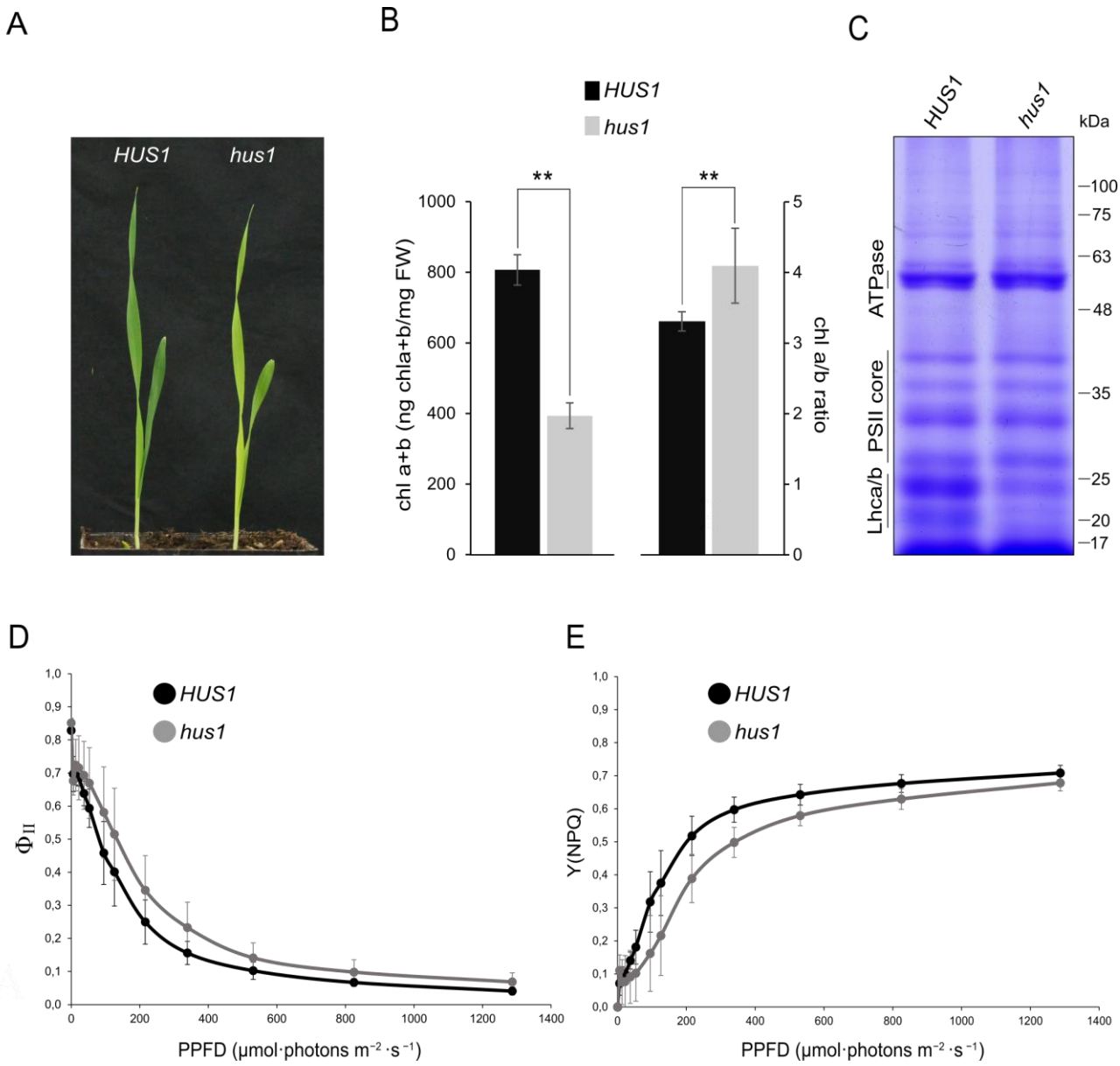

Figure 1. **Phenotypic properties of *HUS1* (control) and *hus1* mutant plants grown under greenhouse conditions**. (**A**) Control barley plants (*HUS1*) and *hus1* mutants (BC_3F_2) were grown for 14 days under controlled greenhouse conditions. (**B**) Contents of chlorophyll a (Chl a) and chlorophyll b (Chl b) in the second leaf, normalized with respect to leaf fresh weight (FW), were quantified by spectrophotometry. Total Chl a+b content and the Chl a/b ratio were determined and statistically validated (Student's t-test, ** $P < 0.01$). Error bars on the histograms indicate standard deviations. (**C**) SDS-PAGE of fractionated thylakoid proteins from second leaves of *HUS1* and *hus1* plants. The

gel was stained with Coomassie Brilliant Blue (C.B.B.). Note the decrease in protein levels in the 20- to 25-kDa range in the *hus1* sample, i.e. in the region of the gel where the antenna proteins of both photosystems (Lhca and Lhcb) migrate. (**D-E**) Light-curve analyses performed using the Dual-PAM 100 fluorometer. The parameters Φ_{II} (the effective quantum yield of PSII) and the quantum yield of regulated energy dissipation of PSII [Y(NPQ)] were measured at increasing light intensities (from dark to 1287 μmol photons m^{-2} s^{-1}; 3 min of exposure to each light intensity). The curves represent the average of three biological replicates and bars indicate standard deviations. PPFD, photosynthetic photon flux density.

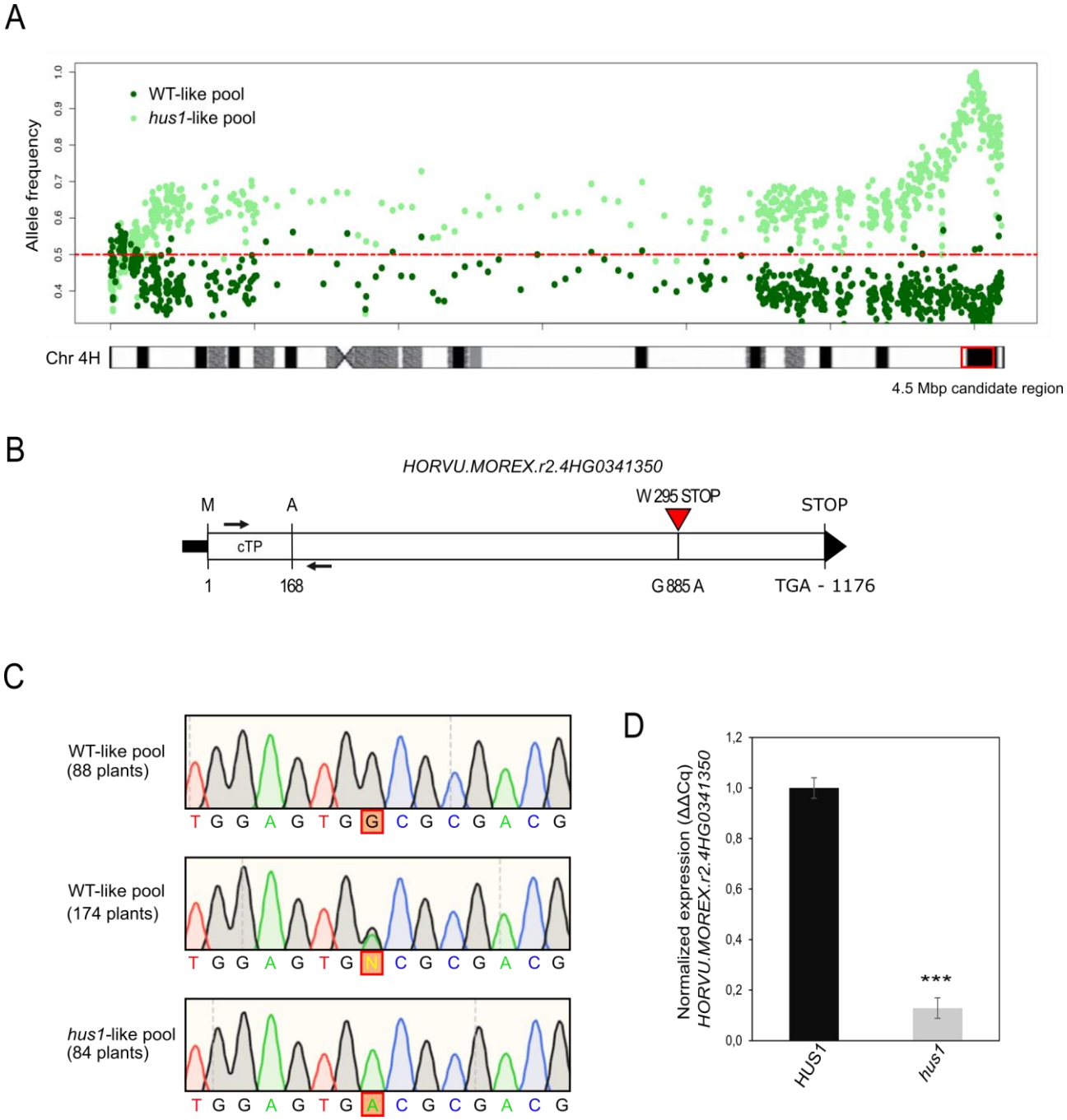

Figure 2. Identification of the *hus1* locus. (**A**) Comparison of allele frequency distributions of exome pools from WT-like (dark green) and *hus1* (pale green) F_2 siblings. Allele frequencies are indicated on the Y axis, genomic coordinates on the X axis together with a karyotype of chromosome 4H. The excess of homozygous alleles at the distal region of the long arm of chromosome 4H corresponds to the 4.5-Mbp candidate region for the *hus1* locus. The red line indicates an allele frequency of 0.5. (**B**) Schematic depiction of *HORVU.MOREX.r2.4HG0341350*. The single-copy gene consists of a single exon, and is predicted to encode a chloroplast transit peptide (cTP) at its 5'-end region [1-to-168 bp from methionine (M) to alanine (A)]. The red triangle indicates the position of the SNP c. G885A mutation [changing a tryptophan (W) codon into a premature stop codon]

identified in this study. The stop codon (TGA) of the wild-type allele c. 1176 is also indicated. Arrows indicate the positions of the primers used for the qRT-PCR reported in (**D**). (**C**) Segregation analysis performed on 346 plants of a Sebastian x *hus1* F_2 population. Only the plants showing the *hus1* phenotype were homozygous for the mutated allele G885A (boxed). (**D**) qRT-PCR performed on *HORVU.MOREX.r2.4HG0341350* transcripts in *HUS1* control and *hus1* mutant leaves. Histograms each represent the average of three technical replicates, and error bars indicate standard deviations (Student's t-test, ***$P<0.001$). Three biological replicates were performed and one representative experiment is shown.

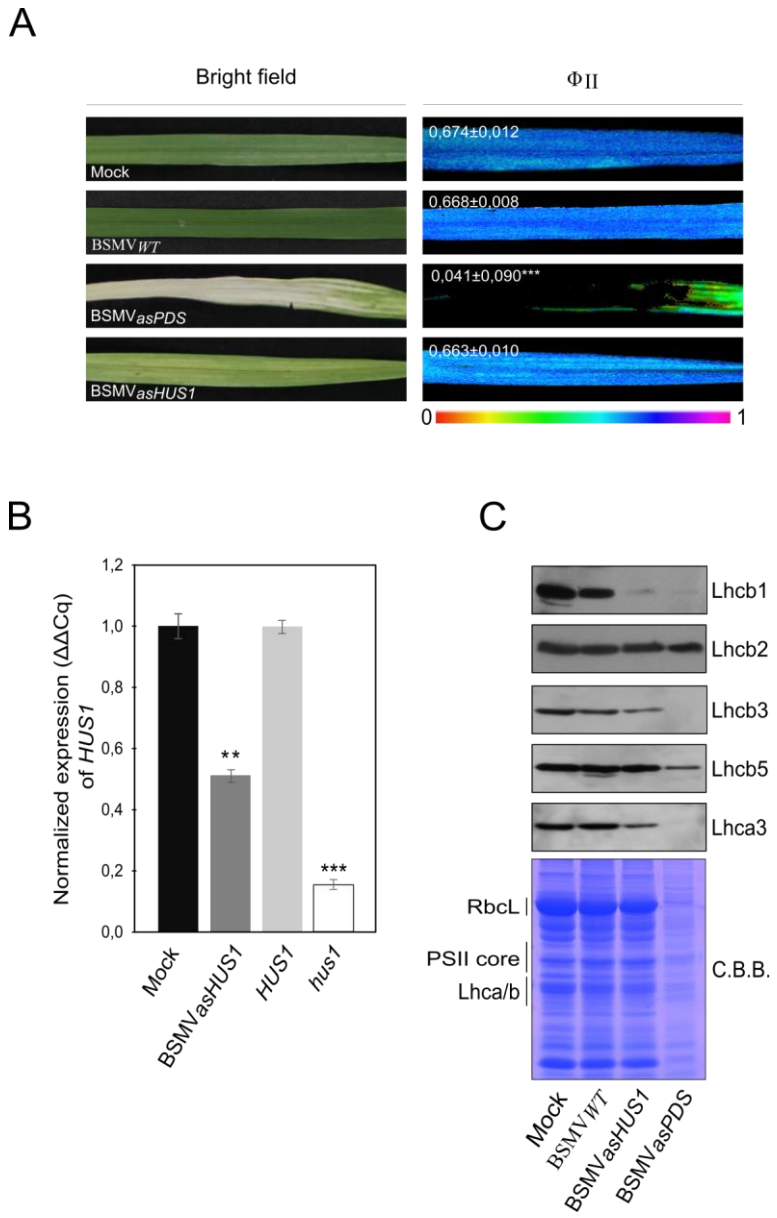

Figure 3. Down-regulation of *HORVU.MOREX.r2.4HG0341350* expression mediated by VIGS. (**A**) Visible phenotypes and photosynthetic parameters of mock-infected (Mock) and BSMV$_{WT}$- BSMV$_{asHUS1}$- and BSMV$_{asPDS}$-infected leaves. Imaging-PAM Φ_{II} values after actinic light exposure (36 µmol photons $m^{-2}\cdot s^{-1}$ for 5 min) are displayed in false colours, violet corresponds to 1 and red to 0. The marked reduction in the Φ_{II} value in the BSMV$_{asPDS}$ line is statistically significant when compared to the other samples (Student's t-test, ***P<0.001). (**B**) qRT-PCR was performed on *HORVU.MOREX.r2.4HG0341350* transcripts from mock-infected (Mock), BSMV$_{asHUS1}$-infected, *HUS1* control and *hus1* mutant leaves. Histograms represent the means of three technical replicates and error bars indicate standard deviations (Student's t-test, **P<0.01, ***P<0.001). Three biological replicates were performed and one representative experiment is shown. (**C**) Immunoblot analysis of total protein extracts (normalized with respect leaf fresh weight) isolated from the indicated sources

with antibodies specific for indicated antenna proteins. One representative filter of three biological replicates is shown. The stained gel (Coomassie Brilliant Blue, C.B.B.) is shown as loading control.

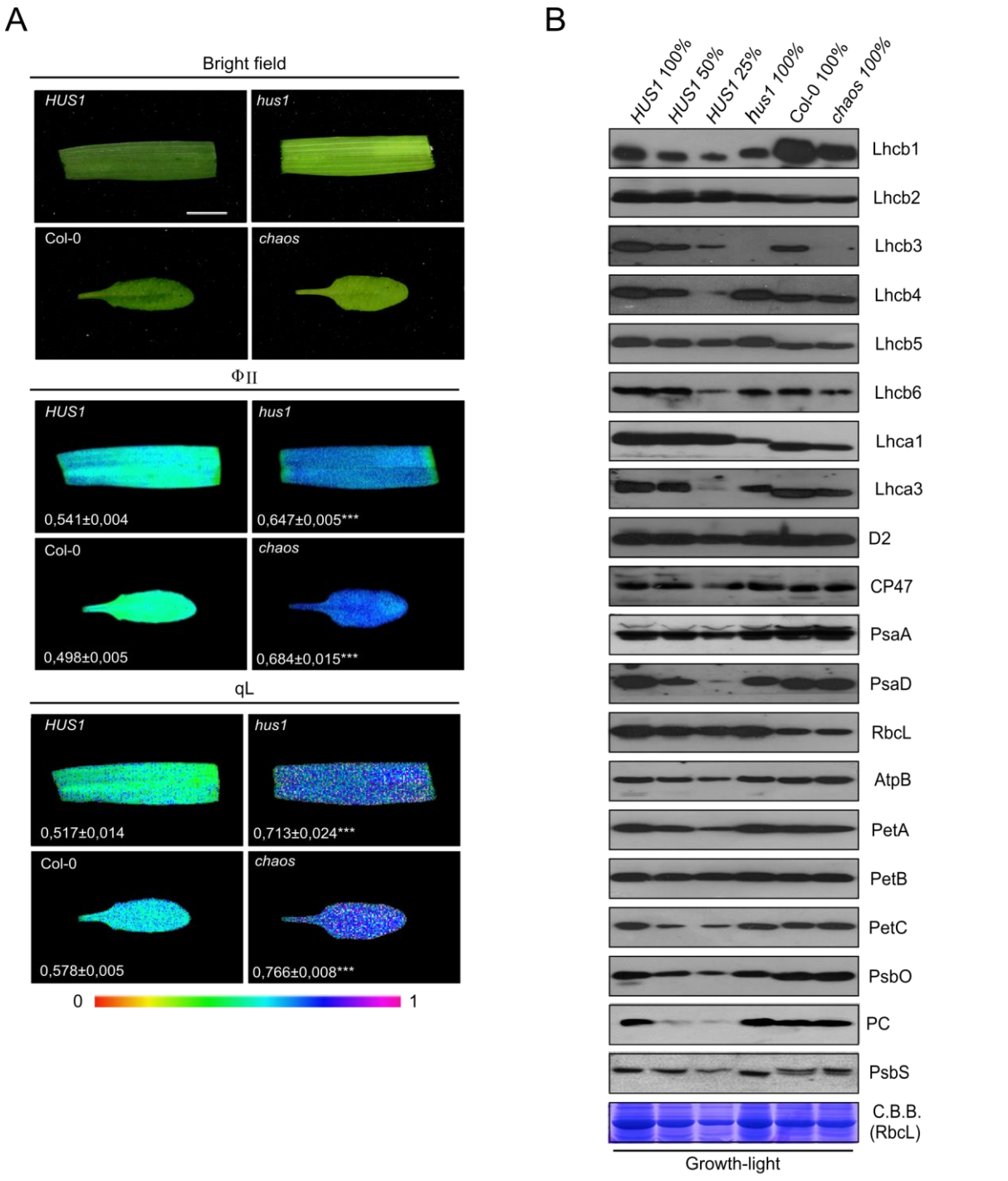
A
Bright field
HUS1
hus1
Col-0
chaos
ΦII
0,541±0,004
0,647±0,005***
0,498±0,005
0,684±0,015***
qL
0,517±0,014
0,713±0,024***
0,578±0,005
0,766±0,008***
0
1
B
HUS1 100%
HUS1 50%
HUS1 25%
hus1 100%
Col-0 100%
chaos 100%
Lhcb1
Lhcb2
Lhcb3
Lhcb4
Lhcb5
Lhcb6
Lhca1
Lhca3
D2
CP47
PsaA
PsaD
RbcL
AtpB
PetA
PetB
PetC
PsbO
PC
PsbS
C.B.B. (RbcL)
Growth-light
C
Col-0
chaos
HUS1
hus1
AtcpSRP43
C.B.B. (RbcL)
D
HUS1
hus1
Col-0
chaos
P-Lhcb1/b2
RbcL
P-Thr
C.B.B.
Dark
Growth-light

Figure 4. Photosynthetic performance and thylakoid protein accumulation in barley *hus1* and Arabidopsis *chaos* mutants. (**A**) Photosynthetic performance of pale-green *hus1* and *chaos* leaves, compared to the corresponding *HUS1* and Col-0 controls. Imaging-PAM values of Φ_{II}, and qL upon a 5-min exposure to actinic light intensities (36 μmol photons m^{-2} s^{-1}) are displayed in false colours. The colour scale is shown below the images, violet corresponds to 1 and red to 0. The differences between control and mutant values of Φ_{II}, and qL parameters are statistically significant (Student's t-test, ***P<0.001). (**B**) Immunoblot analyses of total protein extracts (normalized to leaf fresh weight) from *HUS1*, *hus1*, Col-0 and *chaos* plants with antibodies specific for the indicated proteins of the photosynthetic machinery. For more precise protein quantification, 100%, 50% and 25% dilutions of *HUS1* protein extracts were loaded. (**C**) Immunoblot analyses of total protein extracts (normalized to leaf fresh weight) from Col-0, *chaos*, *HUS1* and *hus1* plants with the antibody specific for *At*cpSRP43. Note that the antibody was unable to recognise *Hv*cpSRP43 protein. (**D**) Total protein extracts from dark- and light-adapted leaves, fractionated by SDS-PAGE and immunodecorated with a phosphothreonine (P-THR) antibody. In panels **B**, **C** and **D** part of the C.B.B-stained gel (corresponding to the RbcL-migrating region) is shown as a control for equal loading. One representative filter of three biological replicates is shown for each immunoblot.

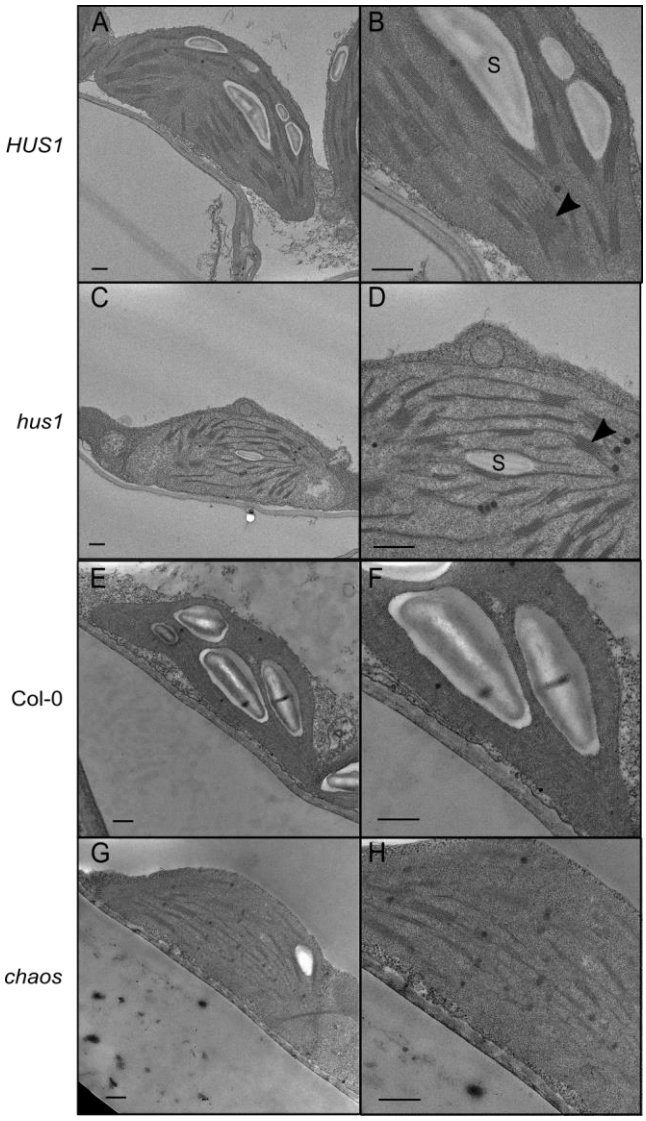

Figure 5. **Analysis of chloroplast ultrastructure by transmission electron microscopy (TEM)**. TEM micrographs showing chloroplast ultrastructure in the *HUS1* control (**a, b**) and the *hus1* barley mutant (**c, d**), and in Arabidopsis Col-0 (**e, f**) and the Arabidopsis *chaos* mutant (**g, h**). The scale-bar = 500 nm. S, starch granule, Arrowheads indicate thylakoid grana stacks.

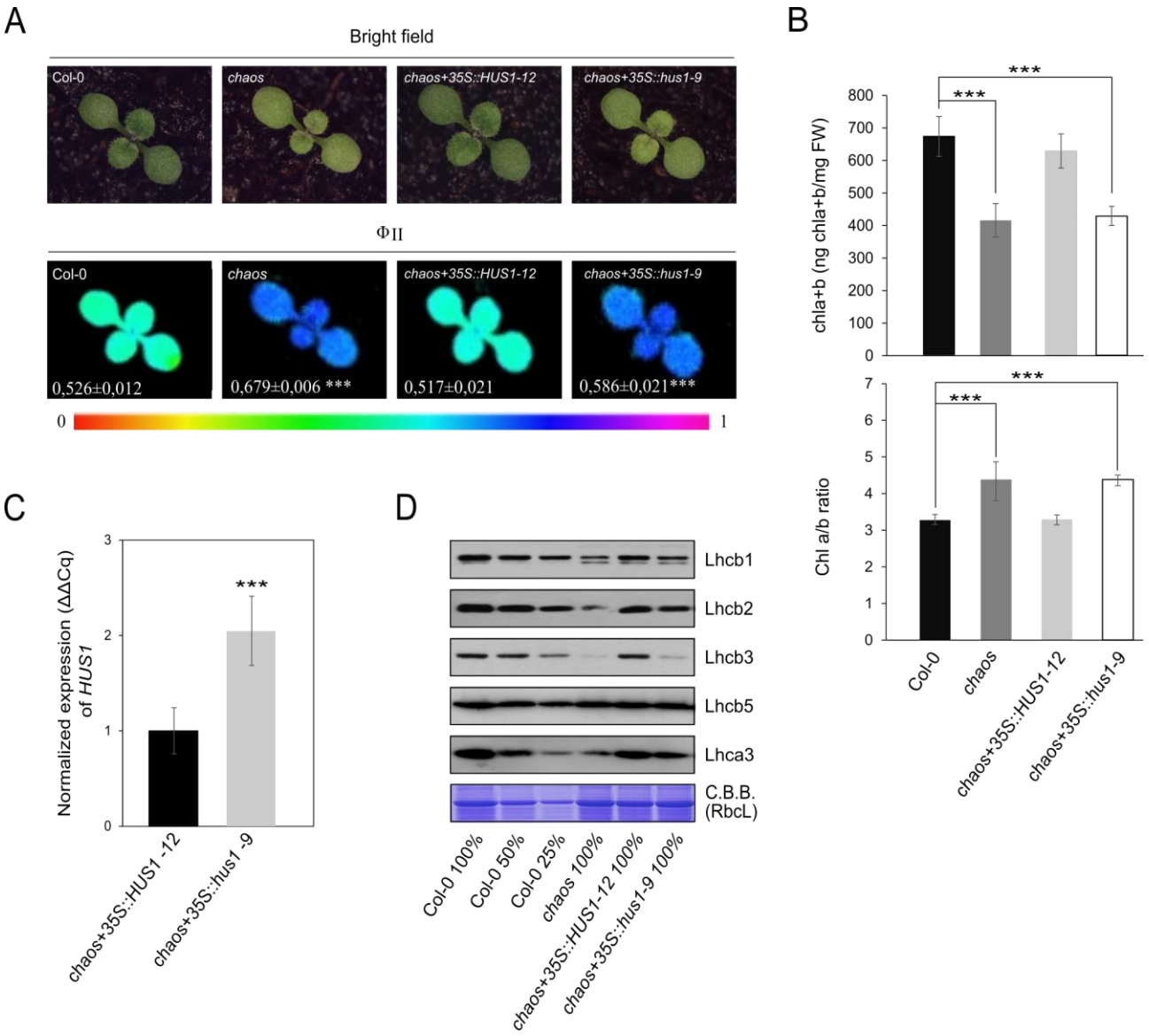

Figure 6. *HORVU.MOREX.r2.4HG0341350* (*HUS1*) rescues the Arabidopsis *chaos* phenotype. (**A**) Visible phenotype and photosynthetic performance of Col-0, *chaos*, *chaos+35S::HUS1-12* T1 line and *chaos+35S::hus1-9* T1 lines at 8 days after sowing. Imaging-PAM values of Φ_{II} after a 5-min exposure to actinic light (36 µmol photons $m^{-2} \cdot s^{-1}$) are displayed in false colours, violet corresponds to the highest photosynthetic efficiency, red to the lowest. The increased Φ_{II} values in the *chaos* and *chaos+35S::hus1-9* lines relative to Col-0 are statistically significant (Student's t-test, ****P*<0.001). (**B**) Chl a+b content and Chl a/b ratio are altered in *chaos* and *chaos+35S::hus1-9* relative to Col-0. Differences are statistically significant (Student's t-test ****P*<0.001). (**C**) qRT-PCR analysis of *HUS1* transcripts in *chaos+35S::HUS1-12* and *chaos+35S::hus1-9* T1 lines. Histograms represent the averages of three technical replicates and error bars indicate standard deviations. Two independent biological replicates were performed and a representative experiment is shown. (**D**) Immunoblot analyses of total protein isolated from Col-0, *chaos*, *chaos+35S::HUS1-12* and

chaos+35S::hus1-9 with antibodies specific for antenna proteins of PSII (Lhcb1 to 3) and PSI (Lhca3), normalized with respect to leaf fresh weight. Note that data for only one of the *chaos+35S::HUS1* and *chaos+35S::hus1* T1 lines are reported. However, similar features were observed in all the other T1 lines. One representative filter of three biological replicates is displayed.

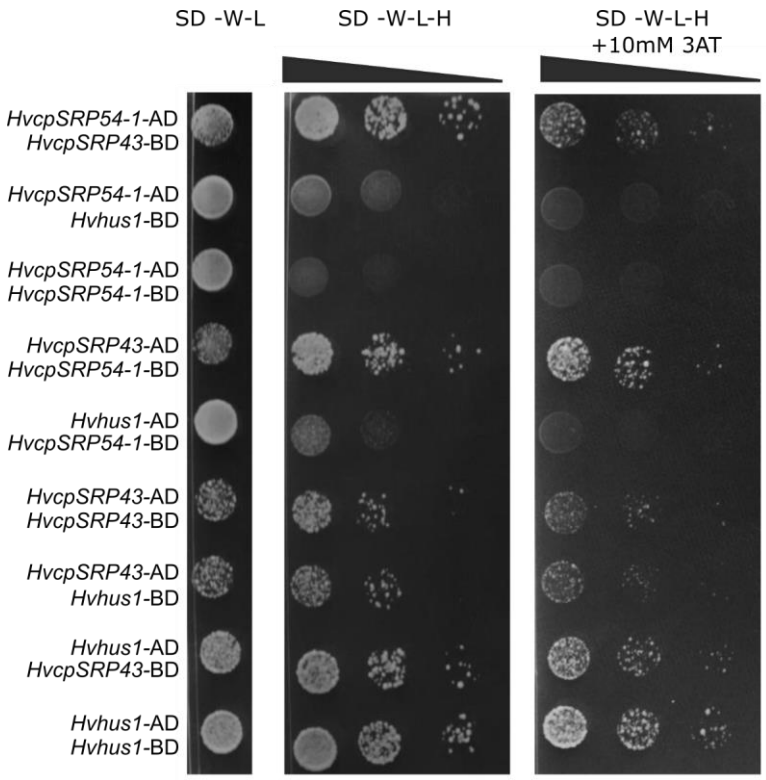

Figure 7. Yeast two-hybrid interaction assay. *Hv*cpSRP43, *Hv*hus1 and *Hv*cpSRP54-1 were tested for physical interaction in both combinations with the GAL4 DNA-binding domain (BD) and the GAL4 activation domain (AD). SD -W -L: Synthetic dropout medium devoid of Trp and Leu (permissive medium); SD -W -L -H: Synthetic dropout devoid of Trp, Leu and His (selective medium) and supplemented with 10 mM 3-AT (3-amino-1,2,4-triazole). Auto-activation tests with the empty vectors (ADØ and BDØ), used as negative controls, are shown in **Figure S4**.

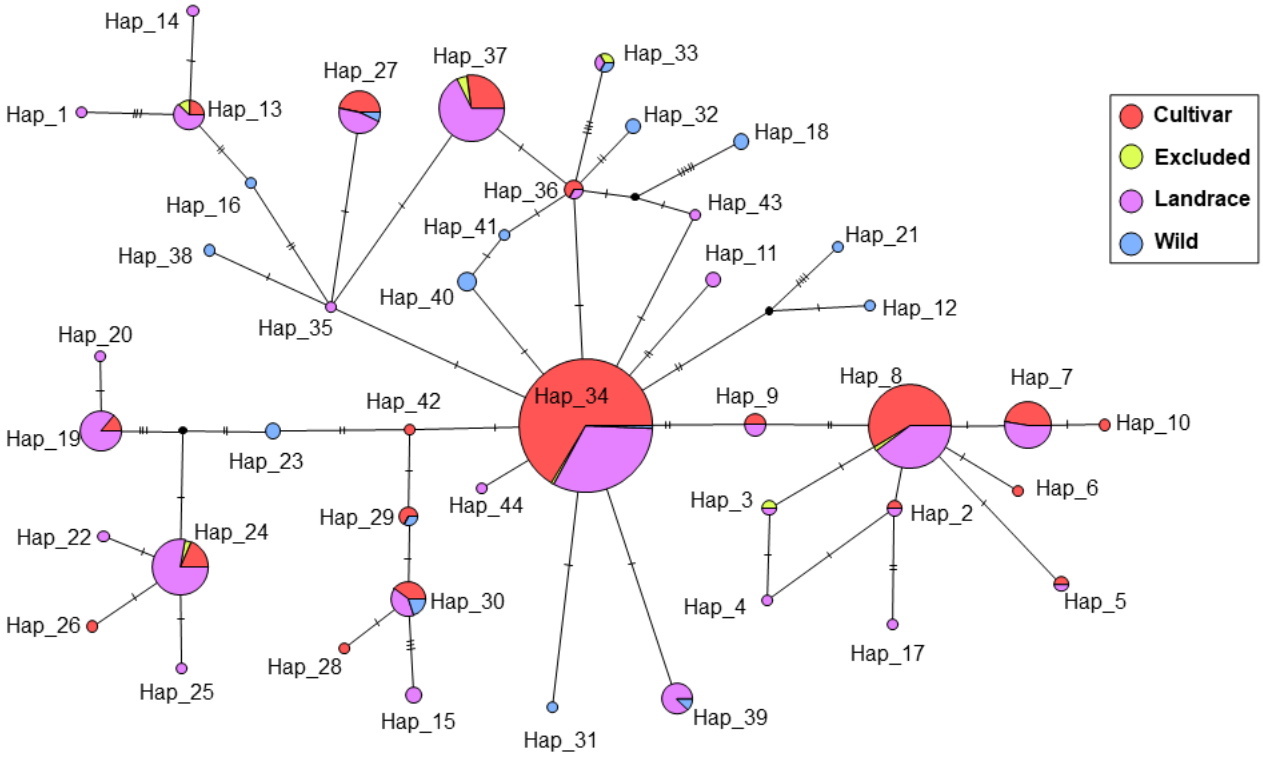

Figure 8. Median-joining haplotype network computed based on haplotypes at *HUS1* retrieved from exome sequencing data of the WHEALBI collection (Bustos-Korts et al., 2019). Haplotypes are represented by circles; circle size is proportional to the number of genotypes per haplotypes. Each circle is colored according to the membership of accessions to one or other of the groups cultivar, landrace and wild. "Excluded" refers to genotypes not used by Bustos-Korts *et al.* (2019) in their analysis. Small ticks in the connector lines represent the numbers of mutations that distinguish the haplotype pairs concerned.

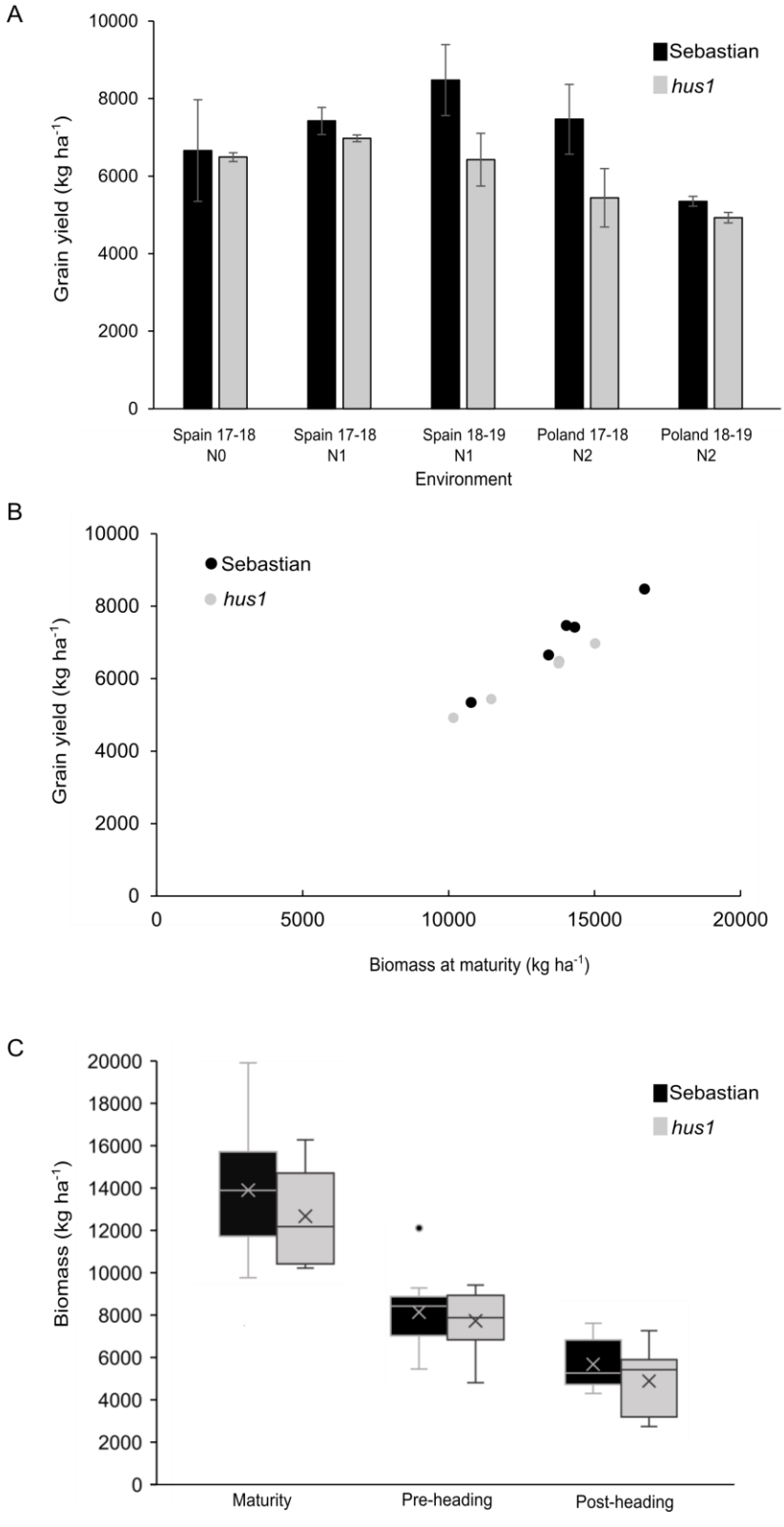

Figure 9. *hus1* and Sebastian plant performance under field conditions.

(**A**) Grain yields observed in *hus1* (gray bars) and Sebastian (black bars) following field trials carried out independently in two successive growing seasons at two different locations. The segment in each bar represents the standard error of the mean. Differences are not statistically significant (Student's

t-test, $P>0.05$). Locations and growing seasons are indicated on the x-axis; N0, no added nitrogen; N1, 150 kg N ha^{-1}; N2, 60 kg N ha^{-1}. (**B**) Relationship between grain yield and total biomass at maturity ($y = 0.52x - 418.9$; $r^2 = 0.91$; $P<0.001$). (**C**) Box plots showing biomass at maturity (DC 92), pre- and post-heading (DC 59) stages for *hus1* (grey boxes) and Sebastian (black boxes) in the five field trials. The horizontal line in each box indicates the median and crosses correspond to the means. The whiskers in each box represent the standard error. Differences are not statistically significant (Student's t-test, $P>0.05$).

Supporting Information

Table S1. List of primers used for PCR-based amplification of DNA and cDNA fragments.

Locus	Gene	Forward primers (5' → 3')	Reverse primers (5' → 3')	Use	Nucleotide at 5' end
HORVU.MOREX.r2.4HG0341350.1	*HvcpSRP43*	AGGTGGAGAAGGTGGTGGAC	TCACCCTGCAAATGTCTCCGCC	G	/
HORVU.MOREX.r2.4HG0341350.1	*HvcpSRP43*	*ATGGAGGCCGTCCTGCGAC	**TCACCCTGCAAATGTCTCCGCC	CA	attB sites
HORVU.MOREX.r2.1HG0001540.1	*HvACTIN 7*	GGGCAGAAGGATGCTTATGT	CCATCACCAGAGTCGAGAAC	RT	/
HORVU.MOREX.r2.4HG0341350.1	*HvcpSRP43*	CTGCGACATCCATCCCTTTC	CTCCTCGTCTTCTTCATCGC	RT	/
HORVU.MOREX.r2.4HG0293270	*HvcpSRP54-1*	GCTGACGAAGGAAACCATTG	GTCGGATTCCTCGGATAACA	RT	/
HORVU.MOREX.r2.4HG0293280	*HvcpSRP54-2*	AAGGTCCCGCTGCCTTCC	CTCCTTTGTCAGTCGATCGA	RT	/
AT2G47450	*AtcpSRP43*	GGACAAGTGCGTAAGGCTTC	CCTCTCTCGTCTTCCACTTC	RT	/
AT5G03940	*AtcpSRP54*	CAGAAGAAGCCAAGTGAGAG	AACTGGGAGACTCACATCTG	RT	/
AT1G13320	*PP2A*	CAGCAACGAATTGTGTTTGG	AAATACGCCCAACGAACAAA	RT	/
HORVU.MOREX.r2.4HG0341350.1	*HvcpSRP43 (AD-Vector)*	GT**GAATTC**GCAGCAAGCAAGGGGGGC	GT**CTCGAG**TCACCCTGCAAATGTCTCC	Y2H	EcoRI/XhoI
HORVU.MOREX.r2.4HG0341350.1	*Hvhus1 (AD-Vector)*	GT**GAATTC**GCAGCAAGCAAGGGGGGC	GT**CTCGAG**TCACCCTGCAAATGTCTCC	Y2H	EcoRI/XhoI
HORVU.MOREX.r2.4HG0293270	*HvcpSRP54-1 (AD-Vector)*	GT**GAATTC**ACGTTCGGGCAGCTCACC AC	GT**GAGCTC**TCAAGGCCTACTGGCGCC AC	Y2H	EcoRI/SacI
HORVU.MOREX.r2.4HG0341350.1	*HvcpSRP43 (BD-Vector)*	GT**GAATTC**GCAGCAAGCAAGGGGGGC	GT**GAATTC**TCACCCTGCAAATGTCTCC	Y2H	EcoRI/EcoRI
HORVU.MOREX.r2.4HG0341350.1	*Hvhus1 (BD-Vector)*	GT**GAATTC**GCAGCAAGCAAGGGGGGC	GT**GAATTC**TCACCCTGCAAATGTCTCC	Y2H	EcoRI/EcoRI
HORVU.MOREX.r2.4HG0293270	*HvcpSRP54-1 (BD-Vector)*	GT**GAATTC**ACGTTCGGGCAGCTCACC AC	GT**GAATTC**TCAAGGCCTACTGGCGCC AC	Y2H	EcoRI/EcoRI
HORVU.MOREX.r2.4HG0341350.1	*HvcpSRP43*	GT**TTAATTAA**CAGAACCCCATCGCCTT ATC	GT**GCGGCCGC**CTCCTCGTCTTCTTCAT CGC	VIGS	PacI/NotI

G, Genotyping; CA, Complementation Assay; RT, Real-time qPCR; Y2H, Yeast two-hybrid; *attB* sites: GGGGACAAGTTTGTACAAAAAAGCAGGCT*; GGGGACCACTTTGTACAAGAAAGCTGGGT**

Asterisks indicate the presence of nucleotide tails at 5'-end needed for the Gateway-based cloning strategy.

Table S2. Quantification of proteins in light-adapted leaves of *HUS1*, *hus1*, Col-0 and *chaos* plants using antibodies specific for proteins of the photosynthetic machinery (see also **Figure 4B**).

Protein	***hus1***	**Col-0**	***chaos***
Lhcb1	0.65±0.11**	3.3±0.21**	2.21±0.33***
Lhcb2	0.19±0.05***	0.17±0.06***	0.15±0.04***
Lhcb3	n.d.	0.55±0.03**	n.d.
Lhcb4	1.02±0.02	0.49±0.04**	0.52±0.05**
Lhcb5	1.04±0.08	0.22±0.05***	0.24±0.04***
Lhcb6	0.44±0.08**	0.52±0.06**	0.29±0.08***
Lhca1	0.11±0.04***	0.19±0.07***	0.12±0.08***
Lhca3	0.39±0.08***	0.98±0.12	0.44±0.06**
D2	1.03±0.12	1.08±0.08	1.06±0.12
CP47	1.16±0.09	0.42±0.05**	0.49±0.06**
PsaA	0.89±0.18	1.33±0.08	1.44±0.12
PsaD	0.79±0.11*	0.95±0.22	0.98±0.14
RbcL	0.94±0.12	0.16±0.04***	0.14±0.05***
AtpB	1.02±0.09	1.08±0.13	0.98±0.18
PetA	0.98±0.18	0.94±0.10	0.97±0.11
PetB	1.03±0.11	1.00±0.08	0.98±0.16
PetC	1.05±0.17	1.04±0.16	1.12±0.13
PsbO	1.08±0.11	1.16±0.12	1.22±0.19
PC	1.15±0.11	1.01±0.09	1.09±0.23
PsbS	0.98±0.14	1.08±0.19	1.04±0.12

HUS1 levels are set to 1 (100%). Values are means ± standard deviation (SD) from three independent protein gel blots. Asterisks indicate statistical significance, as evaluated by Student's t-test and Welch correction (*P<0.05; **P<0.01; ***P< 0.001). n.d., not detected.

Table S3. Statistics of nucleotide and haplotype diversity of the *HUS1* locus in the barley WHEALBI collection.

Parameters	All	Cultivars	Landraces	Wild
Number of samples	403	188	185	22
G+C content	0.63	0.622	0.621	0.622
Number of Haplotypes (h)	44	21	28	16
Haplotype (gene) diversity (Hd)	0.818	0.69	0.875	0.97
Nucleotide diversity (per site) (Pi)	0.00216	0.00174	0.00259	0.00292
Tajima's D	-1.15757	-0.79124	-0.29683	-1.45208

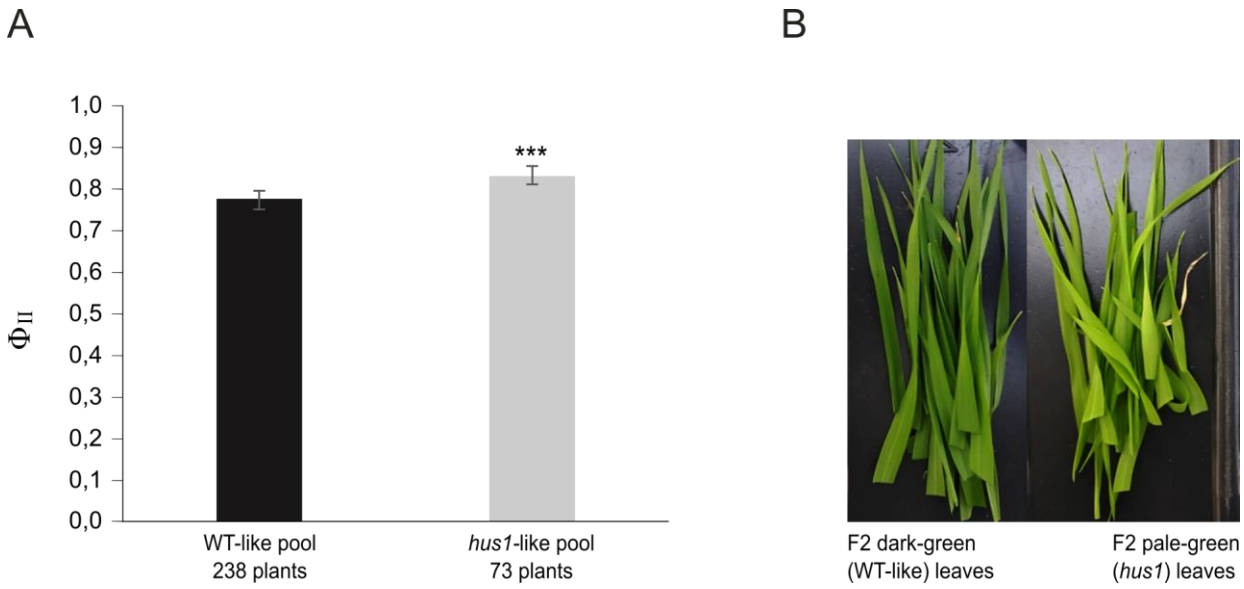

Figure S1 – Segregation analysis of the F_2 offspring of the *hus1* x Morex cross. (**A**) The Φ_{II} parameter was measured with the Handy-PEA fluorimeter in 311 greenhouse-grown plants (see Materials and Methods for details) under low-light conditions (36 μmol photons m^{-2} s^{-1}). 238 plants showed the characteristic Φ_{II} value of around 0.78 ± 0.02, while 73 had an increased photosynthetic performance (Φ_{II} = 0.83 ± 0.03). The latter were also characterised by the pale-green (*hus1*-like) leaf phenotype. Differences between these Φ_{II} values are statistically significant (Student's t-test, ****P*<0.001). Bars indicate standard deviation. The χ^2 (chi-squared test, one degree of freedom) value of 0.386, calculated over the entire F_2 generation (311 plants), indicates that *P*>0.05, validating the hypothesis that the *hus1* phenotype is due to a monogenic recessive allele. (**B**) Leaf phenotype of the two different pools of sibling plants (WT vs *hus1*) used for exome sequencing.

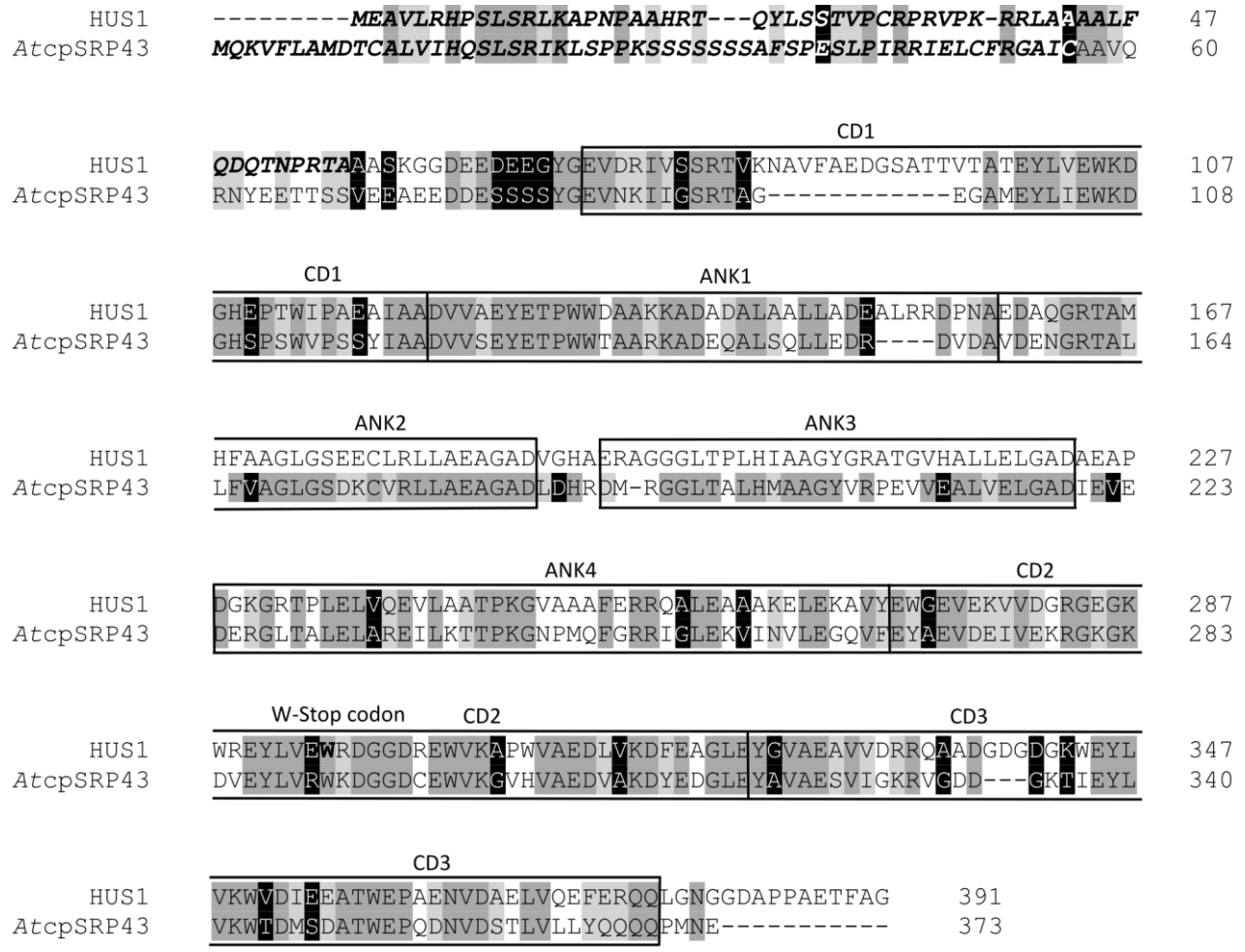

Figure S2 – Comparison of the amino-acid sequences of cpSRP43 from barley and *Arabidopsis thaliana*. Alignment of HUS1 with *At*cpSRP43 using Clustal Omega. The chloroplast transit peptides (cTPs) of the two proteins are indicated in bold italics. Boxes delimit the three chromodomains (CD1 to 3) and the four ankyrin (ANK1 to 3) repeats based on the *Arabidopsis thaliana* protein structure (Stengel *et al.*, 2008). The Trp (W) codon at position 296 in *HUS1* that is changed into a premature stop codon in the *hus1* mutant allele is indicated in bold in CD2. The BLAST alignment reveals 48% (186/384) sequence identity and 62% (241/384) similarity between the two proteins. Conserved amino acids are shown in dark grey, strongly similar residues in light grey and amino acids with weakly similar properties according to Clustal Omega are indicated in black.

A

```
AtcpSRP54       MEALQFSSV--------NRVPCTLSCTG--NRRIKAAFSSAFTGGTINSASLSSSRNLST   50
HvcpSRP54-1     MEATTTLTLSSSPAIAARRSPVRATISQSHLRHC-PVRTSRLH-VACSLA----SR--PL   52
HvcpSRP54-2     MEATATLTLSSSPTG-ARRLPARPAAASLHLRRV-PDLSFRLR-GACCPAAFRALS--SP   55

AtcpSRP54       REIWSWVKSKTVVGHGRYRRSQVRAEMFGQLTGGLEAAWSKLKGEEVLTKDNIAEPMRDI   110
HvcpSRP54-1     SSGWRWRRR--------GSGLVVRAETFGQLTTGLESAWNKLRGVDVLTKETIVEPMRDI   104
HvcpSRP54-2     FPGCRRRRR--------GSGMVVRAEMFGQLTTGLESAWNKLRGVDRLTKENIAEPMRDI   107

AtcpSRP54       RRALLEADVSLPVVRRFVQSVSDQAVGMGVIRGVKPDQQLVKIVHDELVKLMGGEVSELQ   170
HvcpSRP54-1     RRALLEADVSLPVVRRFVSSVSEKALGSDVIRGIRPEQQLVKIVHDELVQLMGGEVSDLV   164
HvcpSRP54-2     RRALLEADVSVPVARSFIESVTEKAVGTDVIRGVQPEQQLVKVVNDELVQLMGGEVSDLV   167

AtcpSRP54       FAKSGPTVILLAGLQGVGKTTVCAKLACYLKKQGKSCMLIAGDVYRPAAIDQLVILGEQV   230
HvcpSRP54-1     FAKTGPTVILLAGLQGVGKTTVCAKLAFYLKKLGKSCMLVAADVYRPAAIDQLTVLGEQV   224
HvcpSRP54-2     FAKTGPTVILLAGLQGVGKTTVCAKLAFYLKKMGKSCMLVAADVYRPAAIDQLTILGKKV   227

AtcpSRP54       GVPVYTAGTDVKPADIAKQGLKEAKKNNVDVVIMDTAGRLQIDKGMMDELKDVKKFLNPT   290
HvcpSRP54-1     GVPVYSEGTTAKPAEITKNAMEEAKRNNIDAIVVDTAGRLQIDKTMMVELKEVKKSVNPT   284
HvcpSRP54-2     GVPVYSEGTEAKPSEIAKNGLKEAKSKKTDVVIVDTAGRLQVDKAMMNELKEVKKAVKPT   287

AtcpSRP54       EVLLVVDAMTGQEAAALVTTFNVEIGITGAILTKLDGDSRGGAALSVKEVSGKPIKLVGR   350
HvcpSRP54-1     EILLVVDAMTGQEAAALVTTFNIEIGISGAILTKLDGDSRGGAALSVKEVSGKPIKFVGR   344
HvcpSRP54-2     EVLLVVDAMTGQEAAALVGAFNVEIGITGAILTKLDGDSRGGAALSIKEVSGKPIKFIGR   347

AtcpSRP54       GERMEDLEPFYPDRMAGRILGMGDVLSFVEKATEVMRQEDAEDLQKKIMSAKFDFNDFLK   410
HvcpSRP54-1     GERMEDLELFYPDRMAQRVLGMGDVLSFVEKAQEVVRQEDTTELQKKIMSAKFDFNDFLK   404
HvcpSRP54-2     GERVEDLEPFYPDRMAQRILGMGDVLSFVEQAQQVMNQEDAEELQKKIMSAKFNFNDFLK   407

AtcpSRP54       QTRAVAKMGSMTRVLGMIPGMGKVSPAQIREAEKNLLVMEAMIEVMTPEERERPELLAES   470
HvcpSRP54-1     QTQNVAKMGSMSRVIGMIPGMNKVTPAQIREAEKRLAFVESMINAMTAEEKEKPELLAES   464
HvcpSRP54-2     QTKAIAQMGSFSRIIGMIPGMNKVTPAQIREAEKNVKFMESMINVMTADERERPELLAES   467

AtcpSRP54       PERRKRIAKDSGKTEQQVSALVAQIFQMRVKMKNLMGVMEGGS-IPALSGLEDALKAEQK   529
HvcpSRP54-1     RERRIRVAEESEKTEQEVSQLVAQLFQMRAQMKKLMGMMQGQPAIAGMGDLMDSLNADEK   524
HvcpSRP54-2     RERRRRVAKDSGKTEQQVSQLVSQLFQMRTRMQKMMAGMQGKDT-PDMETLAESIKSEEQ   526

AtcpSRP54       APPGTARRKRKADSRKK--FVESASSKPGPRGFGSGN   564
HvcpSRP54-1     APPGTARRRRRRSEPPRQRELDAVGGASRP-------   554
HvcpSRP54-2     AAVGTGKRRRK-YGNLRQRDLDSMRGYRR--------   554
```

B

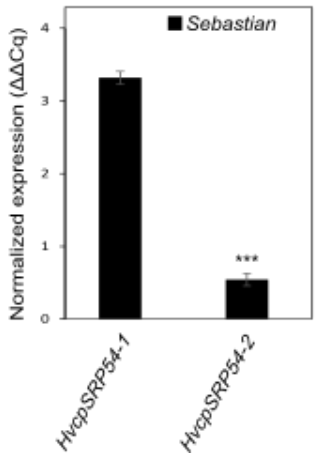

C

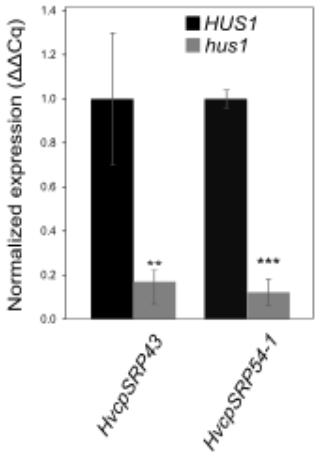

D

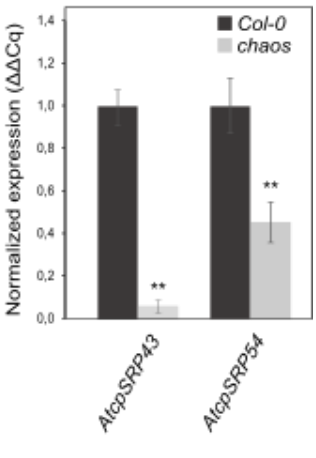

Figure S3 – Amino-acid sequence alignment of barley and Arabidopsis cpSRP54 proteins. (**A**) Multiple alignment between the *Arabidopsis thaliana At*cpSRP54 protein and those encoded by the barley genome, *Hv*cpSRP54-1 and *Hv*cpSRP54-2. N-terminal cTPs are indicated in bold italics. Conserved amino acids are shown in dark grey, strongly similar residues in light grey and amino acids with weakly similar properties according to Clustal Omega are in black. (**B**) Comparative qRT-PCR analysis of *HORVU.MOREX.r2.4HG0293270* (*HvcpSRP54-1*) and *HORVU.MOREX.r2.4HG0293280* (*HvcpSRP54-2*) transcripts in Sebastian. (**C**) qRT-PCR analysis of *HvcpSRP43* and *HvcpSRP54-1* transcripts in Sebastian and *hus1* mutant samples, showing the strict co-regulation of *HvcpSRP43* and *HvcpSRP54-1* gene expression. (**D**) qRT-PCR analysis of *AtcpSRP43* and *AtcpSRP54* transcripts in Col-0 and *chaos* genetic backgrounds, showing a comparable co-regulation pattern between the two genes. qRT-PCR data represent the averages of three technical replicates, and error bars indicate the standard deviationa. Three independent biological replicates were performed and a representative experiment is shown (t-test, $^{**}P<0.01$, $^{***}P< 0.001$).

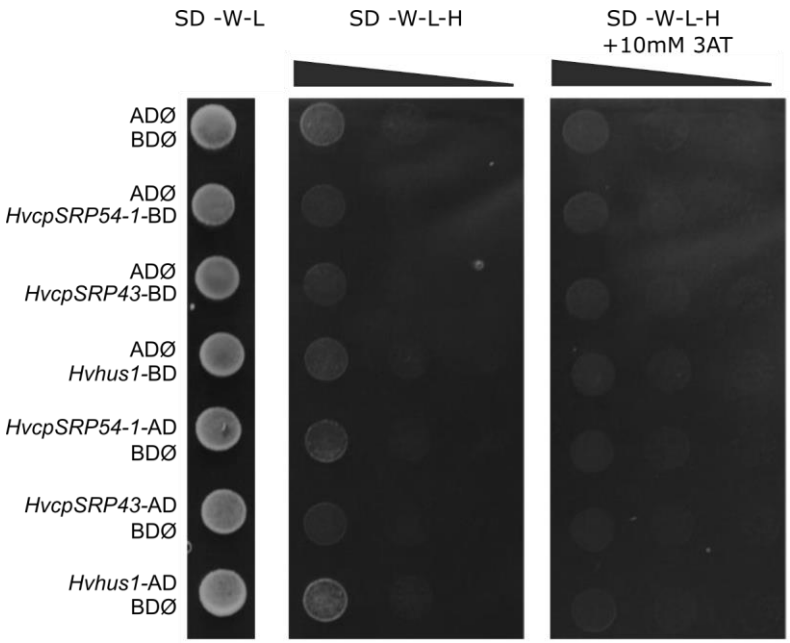

Figure S4 - Yeast two-hybrid interaction assay auto-activation controls. Wild-type *Hv*cpSRP43 (Sebastian), *Hv*cpSRP43 carrying the premature stop codon (*Hv*hus1) and *Hv*cpSRP54-1 were tested for auto-activation in both combinations, i.e. fused to the GAL4 DNA-binding domain (BD) and the GAL4 activation domain (AD), with empty vectors (AD Ø and BD Ø). SD -W -L: Synthetic dropout medium devoid of Trp and Leu (permissive medium); SD -W -L -H: Synthetic dropout medium devoid of Trp, Leu and His (selective medium) and supplemented with 10 mM 3-AT (3-amino-1,2,4-triazole, a histidine biosynthesis inhibitor).

References

Abadia J., Glick R.E., Taylor S.E., Terry N. & Melis A. (1985) Photochemical Apparatus Organization in the Chloroplasts of Two Beta vulgaris Genotypes. *Plant Physiology* **79**, 872–878.

Barbato R., Tadini L., Cannata R., Peracchio C., Jeran N., Alboresi A., … Pesaresi P. (2020) Higher order photoprotection mutants reveal the importance of ΔpH-dependent photosynthesis-control in preventing light induced damage to both photosystem II and photosystem I. *Scientific Reports* **10**, 6770.

Bassi R., Peruffo B., Barbato R. & June R. (1985) Differences in chlorophyll-protein complexes and composition of polypeptides between thylakoids from bundle sheaths and mesophyll cells in maize. *Biochem, J* **595**, 589–595.

Bonardi V., Pesaresi P., Becker T., Schleiff E., Wagner R., Pfannschmidt T., … Leister D. (2005) Photosystem II core phosphorylation and photosynthetic acclimation require two different protein kinases. *Nature* **437**, 1179–1182.

Bustos-Korts D., Dawson I.K., Russell J., Tondelli A., Guerra D., Ferrandi C., … van Eeuwijk F.A. (2019) Exome sequences and multi-environment field trials elucidate the genetic basis of adaptation in barley. *Plant Journal* **99**, 1172–1191.

Campbell B.W., Mani D., Curtin S.J., Slattery R.A., Michno J.M., Ort D.R., Schaus P.J., Palmer R.G., Orf J.H., Stupar R.M. (2015) Identical substitutions in magnesium chelatase paralogs result in chlorophyll-deficient soybean mutants. *G3* **5**, 123–131.

Cingolani P., Platts A., Wang L.L., Coon M., Nguyen T., Wang L., … Ruden D.M. (2012) A program for annotating and predicting the effects of single nucleotide polymorphisms, SnpEff: SNPs in the genome of Drosophila melanogaster strain w1118; iso-2; iso-3. *Fly* **6**, 80–92.

Drewry D.T., Kumar P. & Long S.P. (2014) Simultaneous improvement in productivity, water use, and albedo through crop structural modification. *Global Change Biology* **20**, 1955–1967.

Droppa M., Ghirardi M.L., Horvath G. & Melis A. (1988) Chlorophyll b deficiency in soybean mutants. II. Thylakoid membrane development and differentiation. *Biochimica et Biophysica Acta* **932**, 138–145.

Du S.Y., Zhang X.F., Lu Z., Xin Q., Wu Z., Jiang T., Lu Y., Wang X.F., Zhang D.P. (2012) Roles of the different components of magnesium chelatase in abscisic acid signal transduction. *Plant*

Molecular Biology **80**, 519–537.

Freschet G.T., Dias A.T.C., Ackerly D.D., Aerts R., Van Bodegom P.M., Cornwell W.K., … Cornelissen J.H.C. (2011) Global to community scale differences in the prevalence of convergent over divergent leaf trait distributions in plant assemblages. *Global Ecology and Biogeography* **20**, 755–765.

Funke S., Knechten T., Ollesch J. & Schu D. (2005) A Unique Sequence Motif in the 54-kDa Subunit of the Chloroplast Signal Recognition Particle Mediates Binding to the 43-kDa Subunit. *J Biol Chem* **280**, 8912–8917.

Furbank R.T., Quick W.P. & Sirault X.R.R. (2015) Improving photosynthesis and yield potential in cereal crops by targeted genetic manipulation: Prospects, progress and challenges. *Field Crops Research* **182**, 19–29.

Garrison E. & Marth G. (2012) Haplotype-based variant detection from short-read sequencing. *arXiv:1207.3907*, 1–9.

Genesio L., Bright R.M., Alberti G., Peressotti A., Delle Vedove G., Incerti G., … Miglietta F. (2020) A chlorophyll-deficient , highly reflective soybean mutant : radiative forcing and yield gaps. *Environmental Research Letters* **15**, 074014.

Ghirardi M.L., McCauley S.W. & Melis A. (1986) Photochemical apparatus organization in the thylakoid membrane of Hordeum vulgare wild type and chlorophyll b-less chlorina f2 mutant. *Biochimica et Biophysica Acta (BBA) - Bioenergetics* **851**, 331–339.

Ghirardi M.L. & Melis A. (1988) Chlorophyll b deficiency in soybean mutants. I. Effects on photosystem stoichiometry and chlorophyll antenna size. *Biochimica et Biophysica Acta (BBA)* **932**, 130–137.

Greene B.A., Allred D.R., Morishige D.T. & Staehelin L.A. (1988) Hierarchical Response of Light Harvesting Chlorophyll-Proteins in a Light-Sensitive Chlorophyll b-Deficient Mutant of Maize. *Plant Physiology* **87**, 357–364.

Groves M.R., Mant A., Kuhn A., Koch J., Du S., Robinson C. & Sinning I. (2001) Functional Characterization of Recombinant Chloroplast Signal Recognition Particle. *Journal of Biological Chemistry* **276**, 27778–27786.

Gu J., Zhou Z., Li Z., Chen Y., Wang Z., Zhang H. & Yang J. (2017) Photosynthetic properties and potentials for improvement of photosynthesis in pale green leaf rice under high light

conditions. *Frontiers in Plant Science* **8**, 1082.

Henikoff S., Till B.J., Comai L., Division B.S., Hutchinson F. & Washington S.H. (2004) Perspectives on Translational Biology TILLING . Traditional Mutagenesis Meets Functional Genomics. *Cancer Research* **135**, 630–636.

Holzberg S., Brosio P., Gross C. & Pogue G.P. (2002) Barley stripe mosaic virus -induced gene silencing in a monocot plant. *Plant Journal* **30**, 315–327.

Ihnatowicz A., Pesaresi P., Varotto C., Richly E., Schneider A., Jahns P., … Leister D. (2004) Mutants for photosystem I subunit D of Arabidopsis thaliana : effects on photosynthesis , photosystem I stability and expression of nuclear genes for chloroplast functions. *Plant Journal* **37**, 839–852.

Jensen P.E., Gilpin M. & Scheller H.V. (2000) The PSI-K Subunit of Photosystem I Is Involved in the Interaction between Light-harvesting Complex I and the Photosystem I Reaction Center Core. *J Biol Chem* **275**, 24701–24708.

Jonas-Straube E., Hutin C., Hoffman N.E. & Schünemann D. (2001) Functional Analysis of the Protein-interacting Domains of Chloroplast SRP43. *Journal of Biological Chemistry* **276**, 24654–24660.

Kervestin S. & Jacobson A. (2012) NMD: a multifaceted response to premature translational termination. *Nature reviews. Molecular cell biology* **13**, 700–712.

Kirst H., Garcia-Cerdan J. G., Zurbriggen A., Ruehle T., and Melis A. (2012) Truncated photosystem chlorophyll antenna size in the green microalga *Chlamydomonas reinhardtii* upon deletion of the TLA3-CpSRP43 gene. *Plant Physiology* **160**, 2251–2260.

Kirst H., Melis A. (2013) The chloroplast signal recognition particle (CpSRP) pathway as a tool to minimize chlorophyll antenna size and maximize photosynthetic productivity. *Biotechnol Adv.* **32**, 66–72.

Kirst H., Formighieri C. & Melis A. (2014) Maximizing photosynthetic efficiency and culture productivity in cyanobacteria upon minimizing the phycobilisome light-harvesting antenna size. *Biochimica et Biophysica Acta - Bioenergetics* **1837**, 1653–1664.

Kirst H., Gabilly S.T., Niyogi K.K., Lemaux P.G. & Melis A. (2017) Photosynthetic antenna engineering to improve crop yields. *Planta* **245**, 1009–1020.

Kirst H., Shen Y., Vamvaka E., Betterle N., Xu D., Warek U., … Melis A. (2018) Downregulation

of the CpSRP43 gene expression confers a truncated light-harvesting antenna (TLA) and enhances biomass and leaf-to-stem ratio in Nicotiana tabacum canopies. *Planta* **248**, 139–154.

Klenell M., Morita S., Tiemblo-Olmo M., Mühlenbock P., Karpinski S., Karpinska B. (2005) Involvement of the chloroplast signal recognition particle cpSRP43 in acclimation to conditions promoting photooxidative stress in Arabidopsis. *Plant Cell Physiol.* **46**, 118-29.

Klimyuk V.I., Persello-Cartieaux F., Havaux M., Contard-David P., Schuenemann D., Meiherhoff K., … Nussaume L. (1999) A chromodomain protein encoded by the Arabidopsis CAO gene is a plant-specific component of the chloroplast signal recognition particle pathway that is involved in LHCP targeting. *Plant Cell* **11**, 87–99.

Kogata N., Nishio K., Hirohashi T., Kikuchi S. & Nakai M. (1999) Involvement of a chloroplast homologue of the signal recognition particle receptor protein, FtsY, in protein targeting to thylakoids. **329**, 329–333.

Kramer D.M., Cruz J.A. & Kanazawa A. (2003) Balancing the central roles of the thylakoid proton gradient. *Trends in Plant Science* **8**, 27–32.

Leigh J.W. & Bryant D. (2015) POPART : full-feature software for haplotype network construction. *Methods in Ecology and Evolution 2015* **6**, 1110–1116.

Li H. & Durbin R. (2009) Fast and accurate short read alignment with Burrows – Wheeler transform. *Bioinformatics* **25**, 1754–1760.

Librado P. & Rozas J. (2009) DnaSP v5: A software for comprehensive analysis of DNA polymorphism data. *Bioinformatics* **25**, 1451–1452.

Long S.P., Marshall-Colon A. & Zhu X.G. (2015) Meeting the global food demand of the future by engineering crop photosynthesis and yield potential. *Cell* **161**, 56–66.

Lv X.G., Shi Y.F., Xu X., Wei Y.L., Wang H.M., Zhang X.B., Wu J.L. (2015) Oryza sativa Chloroplast Signal Recognition Particle 43 (OscpSRP43) Is Required for Chloroplast Development and Photosynthesis. *PLoS One*. 10(11):e0143249

Martínez-García J.F., Monte E. & Quail P.H. (1999) A simple, rapid and quantitative method for preparing Arabidopsis protein extracts for immunoblot analysis. *Plant Journal* **20**, 251–257.

Mascher M., Jost M., Kuon J.E., Himmelbach A., Abfalg A., Beier S., … Stein N. (2014) Mapping-by-sequencing accelerates forward genetics in barley. *Genome Biology* **15**, 1–15.

Mascher M., Richmond T.A., Gerhardt D.J., Himmelbach A., Clissold L., Sampath D., … Stein N. (2013) Barley whole exome capture: A tool for genomic research in the genus Hordeum and beyond. *Plant Journal* **76**, 494–505.

Masuda T. & Melis A. (2002) Biosynthesis and Distribution of Chlorophyll among the Photosystems during Recovery of the Green Alga. *Society* **128**, 603–614.

Melis A. (1991) Dynamics of photosynthetic membrane composition and function. *Biochimica et Biophysica Acta Bioenergetics* **1058**, 87–106.

Melis A. (2009) Solar energy conversion efficiencies in photosynthesis: Minimizing the chlorophyll antennae to maximize efficiency. *Plant Science* **177**, 272–280.

Monat C., Padmarasu S., Lux T., Wicker T., Gundlach H., Himmelbach A., … Mascher M. (2019) TRITEX: Chromosome-scale sequence assembly of Triticeae genomes with open-source tools. *Genome Biology* **20**, 284.

Moore M., Harrison M.S., Peterson E.C. & Henry R. (2000) Chloroplast Oxa1p homolog albino3 is required for post-translational integration of the light harvesting chlorophyll-binding protein into thylakoid membranes. *Journal of Biological Chemistry* **275**, 1529–1532.

Mussgnug J.H., Thomas-Hall S., Rupprecht J., Foo A., Klassen V., McDowall A., … Hankamer B. (2007) Engineering photosynthetic light capture: Impacts on improved solar energy to biomass conversion. *Plant Biotechnology Journal* **5**, 802–814.

Nakajima Y. & Ueda R. (1997) Improvement of photosynthesis in dense microalgal suspension by reduction of light harvesting pigments. *Journal of Applied Phycology* **9**, 503–510.

Nakajima Y. & Ueda R. (1999) Improvement of microalgal photosynthetic productivity by reducing the content of light harvesting pigment. *Journal of Applied Phycology* **11**, 195–201.

Negi S., Perrine Z., Friedland N., Kumar A., Tokutsu R., Minagawa J., Berg H., Barry A.N., Govindjee G., Sayre R. (2020) Light regulation of light-harvesting antenna size substantially enhances photosynthetic efficiency and biomass yield in green algae. *Plant Journal* **103**, 584-603.

Okabe K., Schmid G.H. & Straub J. (1977) Genetic Characterization and High Efficiency Photosynthesis of an Aurea Mutant of Tobacco. *Plant Physiology* **60**, 150–156.

Ort D.R., Zhu X., Melis A. (2011). Optimising antenna size to maximize photosynthetic efficiency. *Plant Physiology* **155**, 79-85.

Ort D.R., Merchant S.S., Alric J., Barkan A., Blankenship R.E., Bock R., … Zhu X.G. (2015) Redesigning photosynthesis to sustainably meet global food and bioenergy demand. *Proceedings of the National Academy of Sciences of the United States of America* **112**, 8529–8536.

Paixão J.S., Da Silva J.R., Ruas K.F., Rodrigues W.P., Filho J.A.M., De Paula Bernado W., … Campostrini E. (2019) Photosynthetic capacity, leaf respiration and growth in two papaya (Carica papaya) genotypes with different leaf chlorophyll concentrations. *AoB PLANTS* **11**, 1–15.

Palomar M.K., Brakke M.K. & Jackson A.O. (1977) Base sequence homology in the RNAs of barley stripe mosaic virus. *Virology* **77**, 471–480.

Paro R. & Hogness D.S. (1991) The Polycomb protein shares a homologous domain with a heterochromatin-associated protein of Drosophila. *Proceedings of the National Academy of Sciences of the United States of America* **88**, 263–267.

Pogue G.P., Lindbo J.A., Dawson W.O. & Turpen T.H. (1998) Tobamovirus Transient Expression Vectors: Tools for Plant Biology and High-Level Expression of Foreign Proteins in Plants. In *Plant Molecular Biology Manual*. (ed D. Springer),.

Polle J.E.W., Kanakagiri S.D. & Melis A. (2003) Tla1, a DNA insertional transformant of the green alga Chlamydomonas reinhardtii with a truncated light-harvesting chlorophyll antenna size. *Planta* **217**, 49–59.

Porra R.J., Thompson W.A. & Kriedemann P.E. (1989) Determination of accurate extinction coefficients and simultaneous equations for assaying chlorophylls a and b extracted with four different solvents: verification of the concentration of chlorophyll standards by atomic absorption spectroscopy. *Biochimica et Biophysica Acta* **975**, 384–394.

R Core Team (2018) R: A language and environment for statistical computing. *R Foundation for Statistical Computing*.

Ridgwell A., Singarayer J.S., Hetherington A.M. & Valdes P.J. (2009) Tackling Regional Climate Change By Leaf Albedo Bio-geoengineering. *Current Biology* **19**, 146–150.

Rotasperti L., Sansoni F., Mizzotti C., Tadini L. & Pesaresi P. (2020) Barley's second spring as a model organism for chloroplast research. *Plants* **9**, 1–25.

Sakowska K., Alberti G., Genesio L., Peressotti A., Delle Vedove G., Gianelle D., … Miglietta F.

(2018) Leaf and canopy photosynthesis of a chlorophyll deficient soybean mutant. *Plant Cell and Environment* **41**, 1427–1437.

Schägger H. & von Jagow G. (1987) Tricine-sodium dodecyl sulfate-polyacrylamide gel electrophoresis for the separation of proteins in the range from 1 to 100 kDa. *Analytical Biochemistry* **166**, 368–379.

Schuenemann D., Gupta S., Persello-Cartieauxi F., Klimyuk V.I., Jones J.D.G., Nussaume L. & Hoffman N.E. (1998) A novel signal recognition particle targets light-harvesting proteins to the thylakoid membranes. *Proceedings of the National Academy of Sciences of the United States of America* **95**, 10312–10316.

Schweingruber C., Rufener S.C., Zünd D., Yamashita A. & Mühlemann O. (2013) Nonsense-mediated mRNA decay - Mechanisms of substrate mRNA recognition and degradation in mammalian cells. *Biochimica et Biophysica Acta - Gene Regulatory Mechanisms* **1829**, 612–623.

Seneviratne S.I., Phipps S.J., Pitman A.J., Hirsch A.L., Davin E.L., Donat M.G., … Kravitz B. (2018) Land radiative management as contributor to regional-scale climate adaptation and mitigation. *Nature Geoscience* **11**, 88–96.

Sievers F., Wilm A., Dineen D., Gibson T.J., Karplus K., Li W., … Higgins D.G. (2011) Fast, scalable generation of high-quality protein multiple sequence alignments using Clustal Omega. *Molecular Systems Biology* **7**.

Slattery R.A. & Ort D.R. (2015) Photosynthetic energy conversion efficiency: Setting a baseline for gauging future improvements in important food and biofuel crops. *Plant Physiology* **168**, 383–392.

Slattery R.A., Vanloocke A., Bernacchi C.J., Zhu X.G. & Ort D.R. (2017) Photosynthesis, light use efficiency, and yield of reduced-chlorophyll soybean mutants in field conditions. *Frontiers in Plant Science* **8**, 1–19.

Slattery R.A. & Ort D.R. (2021) Perspectives on improving light distribution and light use efficiency in crop canopies. *Plant Physiology* **185**, 34–48.

Szurman-Zubrzycka M.E., Zbieszczyk J., Marzec M., Jelonek J., Chmielewska B., Kurowska M.M., … Szarejko I. (2018) HorTILLUS—a rich and renewable source of induced mutations for forward/reverse genetics and pre-breeding programs in barley (Hordeum vulgare L.). *Frontiers in Plant Science* **9**, 1–16.

Tadini L., Peracchio C., Trotta A., Colombo M., Mancini I., Jeran N., … Pesaresi P. (2020) GUN1 influences the accumulation of NEP-dependent transcripts and chloroplast protein import in Arabidopsis cotyledons upon perturbation of chloroplast protein homeostasis. *Plant Journal* **101**, 1198–1220.

Tadini L., Romani I., Pribil M., Jahns P., Leister D. & Pesaresi P. (2012) Thylakoid redox signals are integrated into organellar-gene-expression-dependent retrograde signaling in the prors1-1 mutant. *Frontiers in Plant Science* **3**, 1–13.

Tajima F. (1989) Statistical method for testing the neutral mutation hypothesis by DNA polymorphism. *Genetics* **123**, 585–595.

Thielen A.P.G.M. & van Gorkom H.J. (1981) Quantum efficiency and antenna size of Photosystems IIα, IIβ and I in tobacco chloroplasts. *Biochimica et Biophysica Acta (BBA) - Bioenergetics* **635**, 111–120.

Tomiyama M., Inoue S.I., Tsuzuki T., Soda M., Morimoto S., Okigaki Y., Ohishi T., Mochizuki N., Takahashi K., Kinoshita T. (2014) Mg-chelatase I subunit 1 and Mg-protoporphyrin IX methyltransferase affect the stomatal aperture in Arabidopsis thaliana. *J Plant Res* **127**, 553–563.

Tu C., Schuenemann D. & Hoffman N.E. (1999) Chloroplast FtsY , Chloroplast Signal Recognition Particle , and GTP Are Required to Reconstitute the Soluble Phase of Light-harvesting Chlorophyll Protein Transport into Thylakoid Membranes *. *Journal of Biological Chemistry* **274**, 27219–27224.

Verwoerd V., Dekker B.M.M. & Hoekema A. (1989) A small-scale procedure for the rapid isolation of plant RNAs. *Nucleic Acids Research* **17**, 2362.

Wang P., Liang F.C., Wittmann D., Siegel A., Shan S.O. & Grimm B. (2018) Chloroplast SRP43 acts as a chaperone for glutamyl-tRNA reductase, the rate-limiting enzyme in tetrapyrrole biosynthesis. *Proceedings of the National Academy of Sciences of the United States of America* **115**, 3588–3596.

Zadoks J., Chang T. & Konzak C. (1974) A decimal growth code for the growth stages of cereals. *Weed Res* **14**, 415–421.

Zamft B.M. & Conrado R.J. (2015) Engineering plants to reflect light: Strategies for engineering water-efficient plants to adapt to a changing climate. *Plant Biotechnology Journal* **13**, 867–874.

Zhong-wei W., Tian-quan Z., Ya-di X., Xiao-qin Z., Ling W. & Zhong-xian L.I.U. (2016) YGL9 , encoding the putative chloroplast signal recognition particle 43 kDa protein in rice , is involved in chloroplast development. *Journal of Integrative Agriculture* **15**, 944–953.

Ziehe D., Dünschede B. & Schünemann D. (2018) Molecular mechanism of SRP-dependent light-harvesting protein transport to the thylakoid membrane in plants. *Photosynthesis Research* **138**, 303–313.